

Measuring DNA mechanics on the genome scale

<https://doi.org/10.1038/s41586-020-03052-3>

Received: 11 April 2020

Accepted: 21 October 2020

Published online: 16 December 2020

 Check for updates

Aakash Basu^{1,2}, Dmitriy G. Bobrovnikov¹, Zan Qureshi³, Tunc Kayikcioglu^{2,4}, Thuy T. M. Ngo^{2,4}, Anand Ranjan⁵, Sebastian Eustermann^{6,7}, Basilio Cieza³, Michael T. Morgan¹, Miroslav Hejna^{2,8}, H. Tomas Rube^{2,8}, Karl-Peter Hopfner^{6,7}, Cynthia Wolberger¹, Jun S. Song^{2,8,9} & Taekjip Ha^{1,2,3,10,11} 

Mechanical deformations of DNA such as bending are ubiquitous and have been implicated in diverse cellular functions¹. However, the lack of high-throughput tools to measure the mechanical properties of DNA has limited our understanding of how DNA mechanics influence chromatin transactions across the genome. Here we develop ‘loop-seq’—a high-throughput assay to measure the propensity for DNA looping—and determine the intrinsic cyclizabilities of 270,806 50-base-pair DNA fragments that span *Saccharomyces cerevisiae* chromosome V, other genomic regions, and random sequences. We found sequence-encoded regions of unusually low bendability within nucleosome-depleted regions upstream of transcription start sites (TSSs). Low bendability of linker DNA inhibits nucleosome sliding into the linker by the chromatin remodeler INO80, which explains how INO80 can define nucleosome-depleted regions in the absence of other factors². Chromosome-wide, nucleosomes were characterized by high DNA bendability near dyads and low bendability near linkers. This contrast increases for deeper gene-body nucleosomes but disappears after random substitution of synonymous codons, which suggests that the evolution of codon choice has been influenced by DNA mechanics around gene-body nucleosomes. Furthermore, we show that local DNA mechanics affect transcription through TSS-proximal nucleosomes. Overall, this genome-scale map of DNA mechanics indicates a ‘mechanical code’ with broad functional implications.

DNA looping (or cyclization) assays have long been used to measure DNA bendability^{3,4}. Recently, a single-molecule fluorescence resonance energy transfer⁵ (smFRET)-based DNA looping assay was developed⁶, in which the looping of an approximately 100 base-pair (bp) DNA duplex flanked by complementary 10-nucleotide single-stranded overhangs was detected by an increase in FRET between fluorophores located at each end of the DNA (Fig. 1a). The looping rate obtained has been interpreted as a measure of DNA bendability. In the smFRET-based assay, chemically synthesized single strands of DNA had to be annealed directly without PCR amplification to generate a duplex region flanked by long 10-nucleotide overhangs. We simplified the process by developing a nicking-based method that allows the *in situ* conversion of a 120-bp duplex DNA (which can be produced via PCR amplification) into a 100-bp duplex flanked by 10-nucleotide single-stranded overhangs (Fig. 1b). Using FRET⁶, we measured the looping times of ten DNA fragments with different sequences (Supplementary Note 1). The looping times varied by more than an order of magnitude (Fig. 1c), which confirms that the DNA sequence can have a profound effect on DNA looping at the 100-bp length scale, as previously reported^{6,7}. However, looping assays and previous methods to measure DNA bendability directly

have limited throughput, which greatly limits our knowledge of how DNA mechanics is modulated by sequence, varies along genomes, and influences chromosome transactions.

Systematic enrichment of ligands by exponential enrichment (SELEX) has been used to enrich DNA sequences that are more bent⁸ or loopable⁹ through many rounds of selection of rapidly looping DNA and PCR amplification of selected molecules. The distributions of certain periodic dinucleotides in the variable regions of highly loopable DNA have been identified by these assays. However, direct measurements of the bendability of specified sequences of interest, such as those that span genomic regions, have not been reported in high throughput.

To extend direct measurements of DNA bendability to a much larger sequence space, we established a sequencing-based approach termed loop-seq, which builds on previous low-throughput single-molecule looping⁶ and SELEX selection methods⁹. Using the nicking approach, we generated a library of up to approximately 90,000 different specified template sequences immobilized on streptavidin-coated beads. Library members had a central 50-bp duplex region of variable sequence flanked by 25-bp left and right duplex adapters and 10-nucleotide single-stranded complementary overhangs (Fig. 1d).

¹Department of Biophysics and Biophysical Chemistry, Johns Hopkins University School of Medicine, Baltimore, MD, USA. ²Department of Physics, University of Illinois at Urbana-Champaign, Urbana, IL, USA. ³Department of Biophysics, Johns Hopkins University, Baltimore, MD, USA. ⁴Center for Biophysics and Computational Biology, University of Illinois at Urbana-Champaign, Urbana, IL, USA. ⁵Department of Biology, Johns Hopkins University, Baltimore, MD, USA. ⁶Department of Biochemistry, Ludwig-Maximilians-Universität, Munich, Germany. ⁷Gene Center, Ludwig-Maximilians-Universität, Munich, Germany. ⁸Carl R. Woese Institute for Genomic Biology, University of Illinois at Urbana-Champaign, Urbana, IL, USA. ⁹Cancer Center at Illinois, University of Illinois, Urbana, IL, USA. ¹⁰Department of Biomedical Engineering, Johns Hopkins University, Baltimore, MD, USA. ¹¹Howard Hughes Medical Institute, Baltimore, MD, USA.
✉e-mail: tjha@jhu.edu

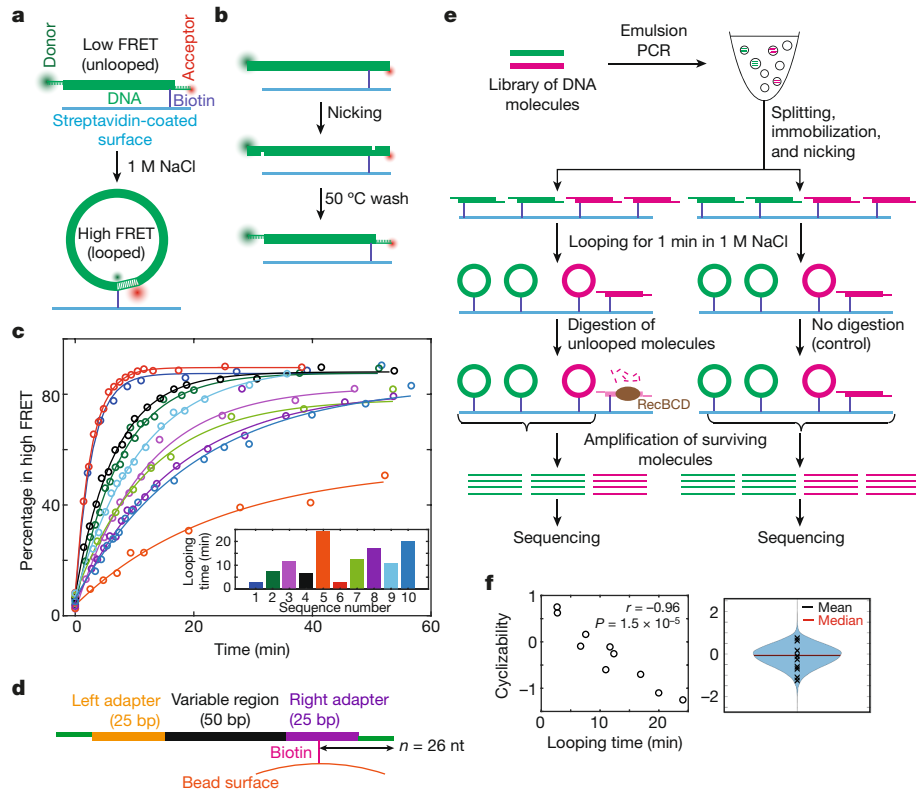


Fig. 1 | A high-throughput method to measure DNA mechanics. **a**, Schematic of the single-molecule looping assay. **b**, In situ nicking of 120-bp duplex DNA 10 nucleotides from either end, followed by washing with buffer at 50 °C, results in the formation of 100-bp duplex molecules flanked by 10-nucleotide single-stranded overhangs (Supplementary Note 1). **c**, Percentage of DNA molecules in the high-FRET (looped) state as a function of time after adding high-salt buffer, for ten DNA sequences (Supplementary Note 1). Inset, looping times (time constants of exponential decay fits (solid lines)). **d**, Schematic of a typical DNA fragment in a library just before looping. n denotes the distance in nucleotides (nt) of the biotin tether from the end of the molecule. **e**, Schematic of loop-seq performed on a hypothetical library comprising only two sequences: green and pink. The library is amplified, immobilized on beads via biotin–streptavidin interactions and nicked in situ to generate loopable

Looping was initiated in high-salt buffer for 1 min, after which unlooped DNA molecules were digested by the RecBCD exonuclease⁹ that requires free DNA ends, thus preserving the looped molecules. The enriched library was sequenced, and the cyclizability of each sequence was defined as the natural logarithm of the ratio of the relative population of that sequence in the enriched library to that in an identically treated control in which the digestion step was omitted (Fig. 1e, Supplementary Note 2).

The looping times of the 10 sequences determined by smFRET (Fig. 1c) were strongly anti-correlated with their cyclizability values obtained by performing loop-seq on a large library containing those 10 (along with 19,897 other) sequences (Fig. 1f). This confirmed that cyclizability is a good measure of looping rate. In addition, varying the time that looping is permitted before RecBCD digestion enabled us to measure the full looping kinetic curves of all sequences in the library (Extended Data Fig. 1, Supplementary Note 3). The looped population could comprise closed structures with alternative shapes and base-pairing geometries^{10,11} (Extended Data Fig. 2). However, irrespective of looped geometry, control experiments indicate that most looped molecules are protected from RecBCD digestion and validate several other aspects of the assay (Extended Data Fig. 3).

We found that the distance of the biotin tether from the end of each molecule (n ; Fig. 1d) imposed an oscillatory modulation on

molecules (d, Methods). After looping for 1 min in high-salt buffer, followed by the digestion of unlooped molecules and amplification of surviving molecules, the relative populations of green and pink in the digested fraction (left) are two-thirds and one-third, respectively. In the control fraction (right), the corresponding values are half and half. The cyclizabilities of green and pink are thus: $\log_e \left(\frac{2}{3} \right)$ and $\log_e \left(\frac{1}{2} \right)$, respectively. **f**, Left, cyclizabilities of two sequences (listed in Supplementary Note 1) that were part of the ‘cerevisiae nucleosomal library’ (see Supplementary Note 4). 95% confidence interval (CI) = −0.99, −0.81. Pearson’s r value is shown. P value determined by two-sided t -test. Right, violin plot of the cyclizabilities of all 19,907 sequences in the cerevisiae nucleosomal library. ‘x’ denotes looping times of the ten sequences measured by smFRET (c).

cyclizability, possibly owing to a sequence-dependent preference for the rotational orientation of the biotin tether (Supplementary Note 7). By varying n and repeating loop-seq several times, we measured the mean, amplitude and phase associated with this oscillation for every library sequence. We called the mean term the ‘intrinsic cyclizability’ and showed that it is independent of the tethering geometry and rotational phasing (Extended Data Fig. 4, Supplementary Notes 7, 8). Both dynamic flexibility and static bending may contribute to intrinsic cyclizability. Regardless of interpretation, intrinsic cyclizability is a measurable mechanical property that can be compared to functional properties of chromosomal DNA.

DNA at yeast nucleosome-depleted regions is rigid

We used loop-seq to determine the role of DNA mechanical properties in establishing characteristic features of genes that regulate expression, such as nucleosome-depleted regions (NDRs) upstream of the TSSs and well-ordered arrays of downstream nucleosomes positioned at characteristic distances from the TSSs¹². Although previous studies have suggested that DNA mechanics, in addition to transcription factors and chromatin remodelers^{2,13,14}, are involved in the regulation of gene expression by altering the organization of nucleosomes^{2,9,15,16}, the mechanical properties of DNA along promoters and genes have

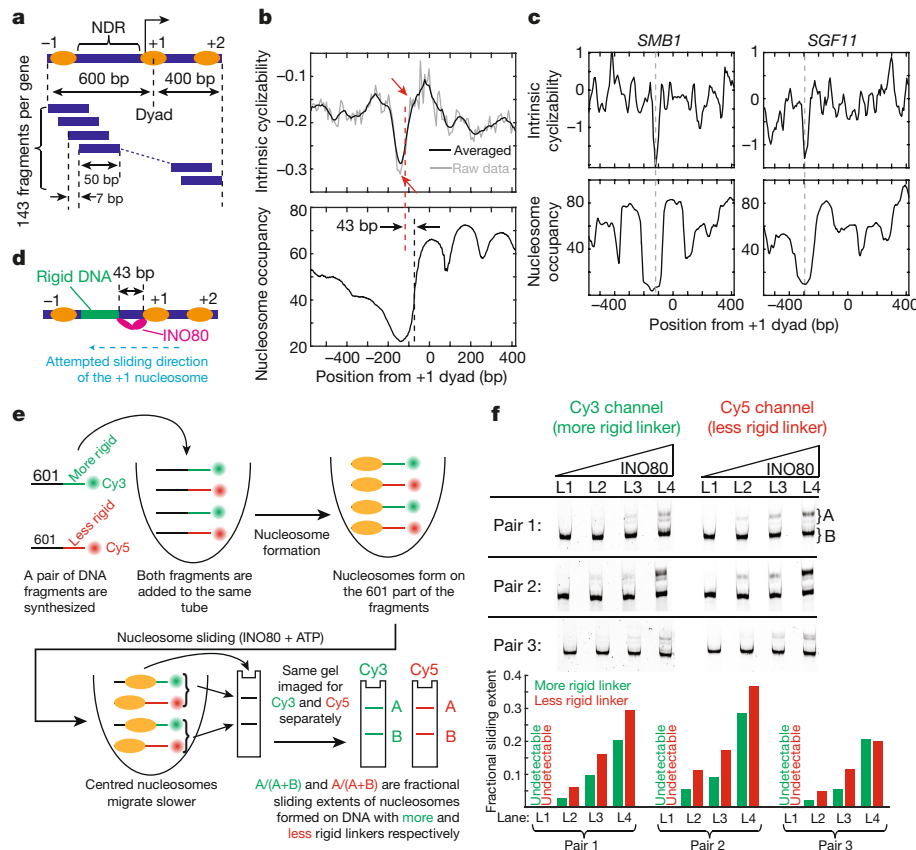


Fig. 2 | DNA mechanics contributes to nucleosome depletion at the NDR and modulates remodeler activities. **a**, Schematic of the tiling library.

The regions around the TSSs of 576 genes were tiled at 7-bp resolution (Supplementary Note 9). DNA, blue bars; nucleosomes, ovals. **b**, Mean intrinsic cyclizability (with (black) and without (grey) any smoothing) (top) and nucleosome occupancy¹⁷ (bottom) versus the position from the canonical location³³ of the dyad of the +1 nucleosome, averaged over all 576 genes in the tiling library. Blue dashed line (at ~73 bp) denotes the edge of the +1 nucleosome; red dashed line denotes the start of the rigid DNA region (approximated as the midpoint between the two red arrows). See Supplementary Note 10. **c**, Intrinsic cyclizability and nucleosome occupancy versus position from the dyads of the +1 nucleosomes of two individual genes (see Extended Data Fig. 5 for more examples). **d**, INO80 attempting to slide a +1 nucleosome upstream of its

canonical location would be poised to contact the rigid DNA region via its Arp8^{21,23}. **e**, Schematic of the experiment comparing the extent of nucleosome sliding by INO80 on a pair of constructs that consist of a nucleosome attached to a rigid or flexible-linker region, and distinguished by different fluorophores (Cy3 and Cy5). Sliding results in centred nucleosomes, which then migrate more slowly on gels²³. See Supplementary Note 11. **f**, Three nucleosome-sliding experiments were performed, involving three pairs of nucleosome constructs as described in **e** and Supplementary Note 11. For each pair, four concentrations of INO80 were used: 2, 6, 9 and 13 nM (lanes L1–L4, respectively). After sliding, nucleosomes were run along a 6% TBE gel, which was imaged separately for Cy3 and Cy5 fluorescence. For each lane, the extent of nucleosome-sliding in the two constructs in the pair was quantified (bar plots). See **e** and Supplementary Note 11.

not been directly measured. We measured the intrinsic cyclizabilities of DNA fragments (Supplementary Note 9) that tile the region from 600 bp upstream to 400 bp downstream of the +1 nucleosome dyads of 576 genes in *S. cerevisiae* at 7-bp resolution (Fig. 2a). We discovered a sharply defined region of rigid DNA (that is, with unusually low intrinsic cyclizability) located in the NDR¹⁷ (Fig. 2b). Furthermore, our measurements are sensitive enough to detect this region of high rigidity in several individual genes (Fig. 2c, Extended Data Fig. 5). As nucleosome assembly requires extensive DNA bending, the low intrinsic cyclizability of DNA around the NDR is likely to favour nucleosome depletion.

Chromatin remodelers sense DNA mechanics

Chromatin remodelers have been proposed to be crucial in establishing the well-ordered array of nucleosomes downstream of TSSs by stacking nucleosomes against a barrier just upstream of the TSS¹⁴. What could constitute such a barrier has been a matter of debate, and transcription factors¹³ and paused polymerases¹⁸ have been suggested to contribute. Notably, chromatin reconstitution experiments *in vitro*² showed that the remodeler INO80 can both position the +1 (and -1) nucleosomes and establish the NDRs in *S. cerevisiae* even in the absence of any such

factors. We therefore asked whether the sequence-encoded rigid DNA region in the NDR can contribute to nucleosome positioning near promoters by serving as a barrier to the sliding activities of INO80.

To effect sliding, INO80 requires at least 40–50 bp of free extranucleosomal DNA ahead of the nucleosome^{19,20}. The region around 40–50 bp ahead of the edge of the sliding nucleosome is engaged by the Arp8 module of INO80^{21–23}, and disrupting the DNA binding of the module by mutation abolishes sliding and reduces +1 positioning genome-wide²³. Notably, we found that the region of rigid DNA also starts around 43 bp upstream of the edge of the +1 nucleosome (Fig. 2b). This would place the Arp8 module in contact with highly rigid DNA if INO80 were to slide the +1 nucleosome upstream from its canonical position (Fig. 2d). If highly rigid DNA interferes with binding of the Arp8 module, further upstream sliding of the +1 nucleosome would be hindered, helping to position the +1 nucleosome and define the NDR.

To directly test the role of upstream DNA rigidity in +1 nucleosome positioning by INO80, we biochemically measured the effect of rigid DNA located approximately 40 bp ahead of a nucleosome. Using a gel-shift assay, we analysed the sliding of nucleosomes formed on the 147-bp 601 sequence into adjacent 80-bp linkers. We chose three pairs of such constructs, each containing one construct with a linker that was

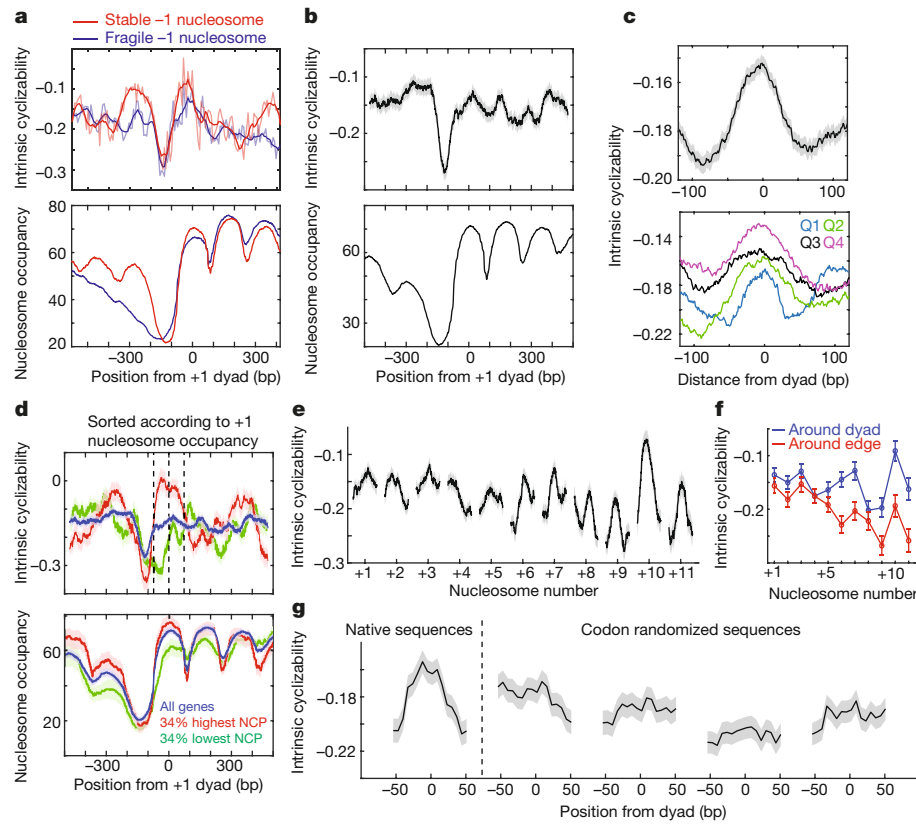


Fig. 3 | DNA mechanics impacts chromosome-wide nucleosome organization. **a, b**, Mean intrinsic cyclizability (top) and nucleosome occupancy (bottom) versus position from the dyad of the +1 nucleosome, averaged over 185 and 345 genes in the tiling library, which possess stable and fragile -1 nucleosomes, respectively²⁵ (plotted as in Fig. 2b) (**a**), and averaged over all 227 identified genes along *S. cerevisiae* chromosome V (Supplementary Note 13) (**b**). Grey background denotes s.e.m. **c**, Intrinsic cyclizability versus position from the dyad, averaged over all 3,192 nucleosomes along chromosome V (top), or over nucleosomes sorted into quartiles (Q1–Q4) based on reported nucleosome centre positioning (NCP) scores³³ (bottom). See also Extended Data Fig. 8a, b. Solid lines denote mean; grey shading denotes s.e.m. **d**, Intrinsic cyclizability (top) and nucleosome occupancy (bottom) (solid lines) versus position along all chromosome V genes (blue), and among 34% of genes with the highest (red) and lowest (green) +1 nucleosome NCP scores³³. Plots

were obtained as in **b**. Dashed lines denote edges and dyad of the +1 nucleosome. Shaded backgrounds denote s.e.m. **e**, Intrinsic cyclizability around nucleosomal dyads that lie within the transcribed region of all identified 227 genes along chromosome V in *S. cerevisiae*. Solid lines denote mean; grey shading denotes s.e.m. See Supplementary Note 13 for *n* values. **f**, Intrinsic cyclizability in a 50-bp window around the dyads (blue) and edges (red, from position -73 till -56 and from +56 till +73) of gene-body nucleosomes as identified in **e**. Data are mean and s.e.m. *N* values as in **e**. **g**, Intrinsic cyclizability of the native sequences around the dyads of the 500 +7 nucleosomes represented in library L (Supplementary Note 14), and along four sets of codon-altered sequences generated by randomly selecting synonymous codons while considering (the first two) or not considering (the next two) the natural codon-usage frequency. Solid line denotes mean, smoothed over a 7-fragment rolling window; grey shading denotes s.e.m.

uniformly flexible and another with a linker that had a considerably more rigid region near the middle (Extended Data Fig. 6a, Supplementary Note 11). In all three pairs, the extent of sliding (Supplementary Note 11) was lower for the nucleosome formed on the construct with the rigid linker (Fig. 2f, Extended Data Figs. 6b, c, 7). Various factors could cause this reduced sliding (Supplementary Note 11). Regardless, the observation is consistent with a model in which the rigid DNA region starting approximately 43 bp upstream of the edge of the canonical +1 nucleosome (Fig. 2b) serves as a barrier that hinders further upstream sliding of the +1 nucleosome by INO80, possibly aided by other barriers set up by factors such as the nucleosome-remodelling complex RSC, gene regulatory factors, and transcription factors^{2,13}. Further studies are needed to define the structural details behind rigidity sensing by the Arp8 module²⁴.

DNA mechanics arranges nucleosomes

As nucleosomes involve extensive DNA bending, we asked whether modulations in intrinsic cyclizability may directly contribute to nucleosome organization, in addition to the stacking action of remodelers¹⁴. Indeed, DNA at the canonical dyad locations of the ±1 nucleosomes,

and to a lesser extent the +2, +3 and +4 nucleosomes, have markedly higher intrinsic cyclizability than surrounding DNA (Fig. 2b). Consistent with this observation, promoters classified as having a fragile -1 nucleosome²⁵ have more rigid DNA at the location of the -1 nucleosome (Fig. 3a).

Several previous studies have shed light on the role of DNA mechanics in nucleosome formation²⁶. The fact that bendable DNA forms good substrates for nucleosomes, and vice versa, has been demonstrated for various selected sequences^{4,27–31}. Furthermore, DNA selected for high loopability from a large random pool possess periodic distribution in dinucleotide contents⁹, which is also a feature found in approximately 3% of native yeast nucleosomal sequences³². However, the mechanical properties of known nucleosomal DNA sequences have not been directly measured in high throughput. To achieve this for nucleosomes along an entire yeast chromosome, we measured the intrinsic cyclizability along *S. cerevisiae* chromosome V at 7-bp resolution (Extended Data Fig. 8, Supplementary Note 12). We first confirmed that intrinsic cyclizability shows the characteristic pronounced dip around the NDR when averaged over the 227 genes along chromosome V that have both ends mapped with high confidence²⁶ (Fig. 3b). We found that chromosome-wide, DNA at nucleosomal dyad locations tends

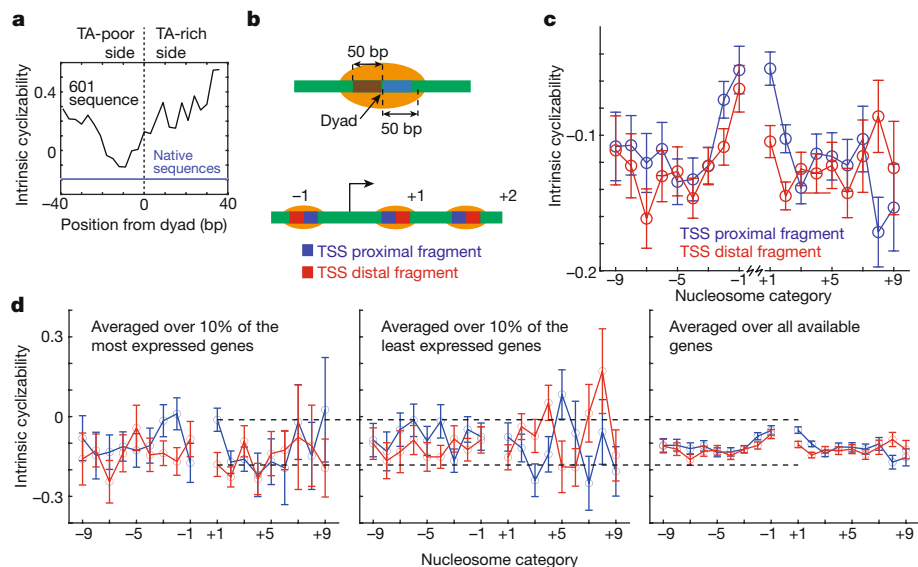


Fig. 4 | TSS-proximal nucleosomes are asymmetric. **a**, Intrinsic cyclizability (black) as a function of position along 601 DNA (Supplementary Note 18). Abscissa value (blue) of the solid horizontal line (-0.196) is the mean intrinsic cyclizability along the 500 native +7 nucleosomal sequences represented in library L (Supplementary Note 14). The height of the light blue background (0.011) is twice the s.e.m. **b**, Schematic representing the design of the cerevisiae nucleosomal library (Supplementary Note 4). The library contains DNA fragments taken from the 50 bp immediately to the left and right of the dyads of the approximately 10,000 nucleosomes (approximately 20,000 50-bp

fragments) in *S. cerevisiae* that have the highest NCP scores. **c**, Mean intrinsic cyclizabilities of the 50-bp DNA fragments that lie immediately adjacent to the TSS proximal (red) or distal (blue) side of the dyads of various categories of nucleosomes (-9 to $+9$) (see Supplementary Note 17). Error bars are s.e.m. See Supplementary Note 17 for the number of nucleosomes in each category over which data was averaged. **d**, A subset of the data in **c**, in which the means were calculated considering only genes among the 10% most (left) or least (middle) expressed in *S. cerevisiae*. The right panel is identical to **c**, except for an altered y-axis scale. Error bars are s.e.m. See Supplementary Note 17.

to have higher intrinsic cyclizability than the surrounding linker DNA (Fig. 3c), which suggests that sequence-dependent modulations in DNA mechanics contribute to global nucleosome organization. We also found that nucleosomes are better positioned *in vivo* on more intrinsically cyclizable DNA (Fig. 3c, Extended Data Fig. 9a–c). Among TSS proximal nucleosomes, the correlation is strongest for +1 nucleosomes (Fig. 3d, Extended Data Fig. 9d, e).

Nucleosomes located at distal downstream regions have a greater difference in intrinsic cyclizability between the dyad and the edges than nucleosomes at promoter-proximal regions (Fig. 3e, f). This is in contrast to expectation, because TSS-proximal nucleosomes are known to be better positioned than TSS-distal nucleosomes^{14,33} and primarily organized by chromatin remodelers into ordered arrays via stacking against the NDR barrier^{2,14}. However, beyond the +4 nucleosome, the stacking effect has been shown to dissipate¹⁴, whereas our data show that modulations in intrinsic cyclizability become more prominent (Fig. 3e, f). Thus, nucleosomes that lie deeper in gene bodies may rely more on sequence-encoded modulations to intrinsic cyclizability for positioning.

DNA mechanics affects codon selection

We next asked whether the strong modulation in intrinsic cyclizability for nucleosomes deep in the gene body would be preserved if the sequences were altered by using alternative codons that code for the same amino acids. We selected 500 +7 nucleosomes in *S. cerevisiae* and generated four sets of codon-altered sequences spanning the region around these nucleosomes, while preserving the amino acid sequences encoded. The natural codon usage frequency was considered when choosing synonymous codons in the first two sets and was ignored in the next two (Supplementary Note 14). By performing loop-seq (Supplementary Note 14), we measured intrinsic cyclizability at 7-bp resolution in the 200-bp region flanking the 500 +7 nucleosome dyads and their codon-altered sequences. Native

sequences have a characteristic intrinsic cyclizability pattern—that is, high near the dyads and low near the edges—which is absent in the four codon-altered sets (Fig. 3g). Thus, naturally occurring codons are optimized to establish sequence-dependent intrinsic cyclizability modulations along genes that are favourable to the organization of gene-body nucleosomes, which suggests that the evolution of codon choice in *S. cerevisiae* has been affected by a selective pressure to preserve such modulations. The observation also points to a hitherto unappreciated importance of positioning nucleosomes that lie deeper in the gene body.

TSS-proximal nucleosomes are asymmetric

Several crucial processes such as transcription and DNA replication require the unravelling of nucleosomes. DNA could potentially peel off from either end, in a manner modulated by bendability. Asymmetry in DNA bendability across the 601 nucleosome leads to asymmetric unravelling under tension³⁴. Biochemical analysis has shown that yeast RNA polymerase II transcribing a 601 nucleosome produces four times more full-length transcripts when it enters the nucleosome through the ‘TA-rich’ side that contains the phased TA repeats³⁵. Using loop-seq, we also found that the TA-rich side has markedly higher intrinsic cyclizability (Fig. 4a, Supplementary Note 18). This observation is consistent with the idea that RNA polymerase might better negotiate with a nucleosomal barrier when it first interacts with the side of the nucleosome that contains DNA with higher intrinsic cyclizability. We constructed a library containing the 50-bp DNA fragments immediately to the left and right of the dyads of approximately 10,000 well-positioned *S. cerevisiae* nucleosomes (Fig. 4b, Supplementary Note 4). We found that DNA at well-occupied +1 and +2 nucleosomes has, on average, higher intrinsic cyclizability on the promoter-proximal face than the distal face (Fig. 4c), which suggests that this asymmetry may favour polymerase translocation. Consistently, this asymmetry is accentuated among the highly expressed genes and absent among poorly expressed genes (Fig. 4d).

Conclusions

Intrinsic cyclizability is, to our knowledge, the only mechanical property of DNA to be directly measured in high throughput, and will improve our understanding of how DNA mechanics influences chromatin transactions involving diverse factors such as topoisomerases, transcription factors, polymerases, and the structural maintenance of chromatin proteins. The large dataset enabled by loop-seq should make it possible to develop comprehensive models to predict intrinsic cyclizability and other physical properties from DNA sequences. Preliminary analysis showed that simple sequence features such as GC content, poly(A) tracts, and dinucleotide parameters are generally weak or insufficient predictors of intrinsic cyclizability (Extended Data Fig. 10, Supplementary Note 16).

Our measurements suggest that intrinsic cyclizability is functionally important and must have applied selective pressure throughout the evolution of genomes. It remains to be determined how genetic information content and the mechanical properties of DNA are linked, and how the sequence-dependent mechanical response of DNA to molecular-scale forces in its immediate environment may have influenced both the slow divergence of organisms and rapid mutations in contexts such as cancer.

Online content

Any methods, additional references, Nature Research reporting summaries, source data, extended data, supplementary information, acknowledgements, peer review information; details of author contributions and competing interests; and statements of data and code availability are available at <https://doi.org/10.1038/s41586-020-03052-3>.

1. Garcia, H. G. et al. Biological consequences of tightly bent DNA: the other life of a macromolecular celebrity. *Biopolymers* **85**, 115–130 (2007).
2. Krietenstein, N. et al. Genomic nucleosome organization reconstituted with pure proteins. *Cell* **167**, 709–721 (2016).
3. Shore, D., Langowski, J. & Baldwin, R. L. DNA flexibility studied by covalent closure of short fragments into circles. *Proc. Natl Acad. Sci. USA* **78**, 4833–4837 (1981).
4. Cloutier, T. E. & Widom, J. Spontaneous sharp bending of double-stranded DNA. *Mol. Cell* **14**, 355–362 (2004).
5. Ha, T. et al. Probing the interaction between two single molecules: fluorescence resonance energy transfer between a single donor and a single acceptor. *Proc. Natl Acad. Sci. USA* **93**, 6264–6268 (1996).
6. Vafabakhsh, R. & Ha, T. Extreme bendability of DNA less than 100 base pairs long revealed by single-molecule cyclization. *Science* **337**, 1097–1101 (2012).
7. Geggier, S. & Vologodskii, A. Sequence dependence of DNA bending rigidity. *Proc. Natl Acad. Sci. USA* **107**, 15421–15426 (2010).
8. Beutel, B. A. & Gold, L. In vitro evolution of intrinsically bent DNA. *J. Mol. Biol.* **228**, 803–812 (1992).
9. Rosanio, G., Widom, J. & Uhlenbeck, O. C. In vitro selection of DNAs with an increased propensity to form small circles. *Biopolymers* **103**, 303–320 (2015).
10. Jeong, J. & Kim, H. D. Base-pair mismatch can destabilize small DNA loops through cooperative kinking. *Phys. Rev. Lett.* **122**, 218101 (2019).
11. Jeong, J. & Kim, H. D. Determinants of cyclization-decyclization kinetics of short DNA with sticky ends. *Nucleic Acids Res.* **48**, 5147–5156 (2020).
12. Lee, W. et al. A high-resolution atlas of nucleosome occupancy in yeast. *Nat. Genet.* **39**, 1235–1244 (2007).
13. Bai, L., Ondracka, A. & Cross, F. R. Multiple sequence-specific factors generate the nucleosome-depleted region on CLN2 promoter. *Mol. Cell* **42**, 465–476 (2011).
14. Zhang, Z. et al. A packing mechanism for nucleosome organization reconstituted across a eukaryotic genome. *Science* **332**, 977–980 (2011).
15. Segal, E. & Widom, J. Poly(dA:dT) tracts: major determinants of nucleosome organization. *Curr. Opin. Struct. Biol.* **19**, 65–71 (2009).
16. Segal, E. et al. A genomic code for nucleosome positioning. *Nature* **442**, 772–778 (2006).
17. Chereji, R. V., Ramachandran, S., Bryson, T. D. & Henikoff, S. Precise genome-wide mapping of single nucleosomes and linkers in vivo. *Genome Biol.* **19**, 19 (2018).
18. Gilchrist, D. A. et al. Pausing of RNA polymerase II disrupts DNA-specified nucleosome organization to enable precise gene regulation. *Cell* **143**, 540–551 (2010).
19. Zhou, C. Y. et al. The yeast INO80 complex operates as a tunable DNA length-sensitive switch to regulate nucleosome sliding. *Mol. Cell* **69**, 677–688.e9 (2018).
20. Brahma, S. et al. INO80 exchanges H2A.Z for H2A by translocating on DNA proximal to histone dimers. *Nat. Commun.* **8**, 15616 (2017).
21. Eustermann, S. et al. Structural basis for ATP-dependent chromatin remodelling by the INO80 complex. *Nature* **556**, 386–390 (2018).
22. Brahma, S., Ngubo, M., Paul, S., Udagama, M. & Bartholomew, B. The Arp8 and Arp4 module acts as a DNA sensor controlling INO80 chromatin remodeling. *Nat. Commun.* **9**, 3309 (2018).
23. Knoll, K. R. et al. The nuclear actin-containing Arp8 module is a linker DNA sensor driving INO80 chromatin remodeling. *Nat. Struct. Mol. Biol.* **25**, 823–832 (2018).
24. Oberbeckmann, E. et al. Genome information processing by the INO80 chromatin remodeler positions nucleosomes. Preprint at <https://doi.org/10.1101/2020.11.03.366690> (2020).
25. Kubik, S. et al. Nucleosome stability distinguishes two different promoter types at all protein-coding genes in yeast. *Mol. Cell* **60**, 422–434 (2015).
26. Widom, J. Role of DNA sequence in nucleosome stability and dynamics. *Q. Rev. Biophys.* **34**, 269–324 (2001).
27. Drew, H. R. & Travers, A. A. DNA bending and its relation to nucleosome positioning. *J. Mol. Biol.* **186**, 773–790 (1985).
28. Hayes, J. J., Tullius, T. D. & Wolffe, A. P. The structure of DNA in a nucleosome. *Proc. Natl Acad. Sci. USA* **87**, 7405–7409 (1990).
29. Widlund, H. R. et al. Nucleosome structural features and intrinsic properties of the TATAAACGCC repeat sequence. *J. Biol. Chem.* **274**, 31847–31852 (1999).
30. Shrader, T. E. & Crothers, D. M. Artificial nucleosome positioning sequences. *Proc. Natl Acad. Sci. USA* **86**, 7418–7422 (1989).
31. Lowary, P. T. & Widom, J. New DNA sequence rules for high affinity binding to histone octamer and sequence-directed nucleosome positioning. *J. Mol. Biol.* **276**, 19–42 (1998).
32. Jin, H., Rube, H. T. & Song, J. S. Categorical spectral analysis of periodicity in nucleosomal DNA. *Nucleic Acids Res.* **44**, 2047–2057 (2016).
33. Brogaard, K., Xi, L., Wang, J.-P. & Widom, J. A map of nucleosome positions in yeast at base-pair resolution. *Nature* **486**, 496–501 (2012).
34. Ngo, T. T. M., Zhang, Q., Zhou, R., Yodh, J. G. & Ha, T. Asymmetric unwrapping of nucleosomes under tension directed by DNA local flexibility. *Cell* **160**, 1135–1144 (2015).
35. Bondarenko, V. A. et al. Nucleosomes can form a polar barrier to transcript elongation by RNA polymerase II. *Mol. Cell* **24**, 469–479 (2006).

Publisher's note Springer Nature remains neutral with regard to jurisdictional claims in published maps and institutional affiliations.

© The Author(s), under exclusive licence to Springer Nature Limited 2020

Article

Methods

No statistical methods were used to predetermine sample size. The experiments were not randomized, and investigators were not blinded to allocation during experiments and outcome assessment.

smFRET based single-molecule DNA looping assay

Templates were purchased (IDT DNA) and converted into loopable molecules with 10 bp complementary overhangs on either side, Cy3 and Cy5 fluorophores at the ends, and a biotin molecule (Supplementary Note 1) via PCR amplification with KAPA Hi Fi Polymerase (Roche) and nicking near the ends by the site-specific nicking enzyme Nt.BspQ1 (NEB). Molecules were immobilized on a PEG-coated quartz surface (JHU slide production core for microscopy) functionalized with a small amount of biotin-PEG, via a streptavidin sandwich, as previously described⁶. Immobilized molecules were incubated with T2.5 (2.5 mM NaCl, 10 mM Tris-HCl pH 8) for 1.5 h. Low-salt imaging buffer (20 mM Tris-HCl pH 8, 3 mM Trolox, 0.8% dextrose, 0.1 mg ml⁻¹ glucose oxidase, 0.02 mg ml⁻¹ catalase) was flowed into the channel and the molecules were imaged on a TIRF microscope to determine the initial histogram of FRET values. High-salt imaging buffer (1 M NaCl, and all components of the low salt imaging buffer) was then introduced into the channel at time 0, and FRET histograms were measured at various time points as done previously⁶. The plot of the percentage of molecules with both donor–acceptor pairs in high FRET as a function of time was fit to an exponential. Its time constant was defined as the looping time. The inverse of this was defined to be the looping rate.

Loop-seq

Instead of individual templates, entire libraries representing as many as approximately 90,000 individual DNA sequences, with the central 50 bp variable and flanked by identical 25 bp adapters, were obtained (Genscript), and amplified using KAPA Hi Fi polymerase (Roche) in 20 cycles of emulsion PCR³⁶ (ePCR) using the MicellaDNA emulsion and purification kit (CHIMERx). The manufacturer's guidelines were followed during ePCR. ePCR prevents improper annealing among different template molecules via the common adaptor sequences. Amplification converted the library into 120 bp duplex molecules with a biotin near one end, and the recognition sequence for the nicking enzyme Nt.BspQ1 (NEB) near both ends (Supplementary Note 1). Twenty microliters of streptavidin-coated magnetic beads (Dynabeads MyOne Streptavidin T1, Thermo Fisher Scientific) was washed twice with 400 µl T50 BSA (1 mg ml⁻¹ BSA (Invitrogen) in T50 (50 mM NaCl, 10 mM Tris-HCl pH 8.0)) and resuspended in 20 µl T50 BSA. Amplified DNA (2 µl of approximately 4 ng µl⁻¹) was mixed with 5 µl of water, and 20 µl of the washed magnetic beads were added. After incubation for 10 min, the DNA-bound beads were washed twice with 200 µl T50BSA and once with 200 µl T10BSA (1 mg ml⁻¹ BSA (Invitrogen) in T10 (10 mM Tris-HCl pH 8.0, 10 mM NaCl)). Digestion mix (84 µl water, 10 µl 10× NEB buffer 3.1, 6 µl Nt.BspQ1 (NEB)) was prepared and heated to 50 °C for 5 min. Digestion resulted in an immobilized library, in which every DNA molecule has a central 50-bp duplex variable region, flanked by 25-bp left and right adapters and 10-nucleotide complementary single-stranded overhangs (Fig. 1d, Supplementary Note 1). The beads were pulled down and incubated with the heated digestion mix for 25 min at 37 °C. The beads were then washed twice with 100 µl of T10BSA preheated to 50 °C, followed by 200 µl of T2.5BSA (1 mg ml⁻¹ BSA (Invitrogen) in T2.5 (10 mM Tris-HCl pH 8.0, 2.5 mM NaCl)). The beads were incubated in 200 µl T2.5BSA for 1.5 h on a rotor at room temperature. The bead sample was then split into two 95 µl fractions denoted 'sample' and 'control'. The beads in the sample fraction were pulled down and resuspended in 200 µl looping buffer (1 M NaCl, 1 mg ml⁻¹ BSA, 10 mM Tris-HCl pH 8) for 40 s. High-salt buffer (1 M NaCl) initiates looping, which allows the complementary single-stranded overhangs at the ends to stably hybridize⁶. Apparent DNA bendability has been shown

to be independent of the salt concentration used⁶. The tube containing the sample was then placed on magnets for an additional 35 s. The looping buffer was replaced with 200 µl of digestion buffer (6.66 µl of RecBCD (NEB), 20 µl 10× NEB buffer 4, 20 µl of 10× ATP (NEB), 154 µl water) for 20 min. This was defined as looping for 1 min. In general, looping for *n* minutes indicates incubation in looping buffer for up to 20 s before the completion of *n* minutes, followed by 35 s over magnets before the solution was replaced with digestion buffer. After 20 min, digestion buffer was removed by pulling down the beads and replaced with 200 µl of looping buffer. The control was treated in exactly the same way, except the digestion buffer had 6.66 µl of water instead of RecBCD. Beads in the sample and control fractions were then pulled down and the looping buffer was replaced with 50 µl of PCR mix (25 µl 2× HiFi KAPA Hot Start ready mix (Roche), 1 µl each of 100 µM primers (Supplementary Note 1), 23 µl water) and PCR amplified (16 cycles). If the library contained less than 20,000 sequences, the products were sequenced on an Illumina MiSeq machine. For more complex libraries a HiSeq machine was used. Library preparation for sequencing was done using the Nextera XT primer kit and followed a protocol similar to the Illumina protocol for 16S metagenomic sequencing library preparation.

Sequencing results were mapped to the known sequences in the library using Bowtie 1³⁷. The number of times each sequence was represented in the sample and control was obtained and 1 was added to all counts. The relative population of each sequence in the digested and control pools was calculated. Cyclizability of a sequence was defined as the natural logarithm of the ratio of the relative population of a sequence in the sample pool to that in the control. In addition to Bowtie 1³⁷, SAMtools³⁸, smCamera, and MATLAB (MathWorks) versions 9.0, 9.2, 9.4, 9.6 were used to analyse the data.

Purification of INO80

INO80 was purified according to a protocol published earlier³⁹. In brief, *S. cerevisiae* cells were grown in 1 l of YPD medium to an optical density (OD) of 1.5. Frozen yeast cells were lysed in a SPEX freezer mill (15 cycles: precool 2 min, run time 1 min, cool time 1 min, rate 15 cps). INO80-3Flag was affinity-purified from whole lysate using anti-Flag M2 agarose beads and eluted with Flag peptide (0.5 mg ml⁻¹). The complex was further purified by sedimentation over a 20–50% glycerol gradient. Peak INO80 fractions were pooled and concentrated using Centricon filters (50 kDa cut off), and buffer changed to 25 mM HEPES-KOH (pH 7.6), 1 mM EDTA, 2 mM MgCl₂, 10% glycerol, 0.01% NP-40, 0.1 M KCl. Aliquots of purified INO80 were flash-frozen and stored at -80 °C. Recombinant INO80 was also purified as per earlier protocols²¹.

Nucleosome sliding by INO80

Nucleosome preparation and sliding by INO80 was performed under conditions as reported earlier¹⁹. Sliding in the presence of various concentrations of INO80 as reported in Fig. 2f (for 1 min) and Extended Data Fig. 7 (for 1 min and 2.5 min) was performed in 10 µl reaction volumes containing 8 nM nucleosomes (nucleosomes formed on both constructs in the pair were present in equimolar proportion), 2 mM ATP, 24 mM Tris-HCl pH 7.5, 43 mM KCl, 2.86 mM MgCl₂, 0.55% glycerol and indicated concentration of INO80. The mixture was incubated without ATP at 30 °C for 7 min. After addition of ATP, the reaction was allowed to proceed for 1 min at 30 °C, and was then quenched by the addition of lambda DNA and ADP to final concentrations of 66.7 µg ml⁻¹ and 20 mM respectively. For all sliding experiments reported in Extended Data Fig. 6b (time course of INO80 sliding), conditions were the same except incubations before ATP addition and the subsequent sliding reaction were carried out at room temperature. The reaction was continued for the indicated amounts of time in presence of saturating INO80 before quenching. Quenched reactions were loaded on to 6% TBE (Tris-borate-EDTA) gels (Invitrogen) in presence of 10% glycerol and run at 150 V for 1.5 h. The gel was imaged separately for Cy3 and Cy5 fluorescence.

Statistics and reproducibility

All presented loop-seq data in figures (unless explicitly comparing between multiple loop-seq runs on the same library, as in Extended Data Fig. 3c) were compiled from a single run of loop-seq on the library in question. However, some sequences in every library were included as part of at least one other library. Pearson's coefficient of correlation for the intrinsic cyclizability values of these common sequences (and the 95% confidence interval and *P* values), as obtained via the two independent loop-seq runs on the two libraries, was measured to confirm reproducibility (Extended Data Fig. 3a–c, Supplementary Notes 4–6, 9, 12, 14). All such Pearson's correlation coefficients were greater than or similar to the correlation coefficient of cyclizability values of the two sets of reverse complement sequences in the 'mixed reverse complement of the random library and the random library' (Extended Data Fig. 3f). Furthermore, measurements of intrinsic cyclizabilities of common sequences in different libraries constitute completely independent measurements starting from independently purchased libraries from the manufacturer.

All Pearson's *r* values have been calculated using the 'corrcoef' function in MATLAB (MathWorks). For two random variables A and B, Pearson's *r* is the covariance of A and B, divided by the product of their standard deviations. *P* values have always been calculated using the MATLAB (MathWorks) function 'corrcoef', which calculates the *P* value by transforming the correlation to create a *t*-statistic having *n* – 2 degrees of freedom, where *n* is the number of measurements. The test was always two-sided. Further, extremely small *P* values have always been indicated as *P* < 0.00001.

Reproducibility of the result that nucleosome sliding by INO80 is favoured by flexible linker DNA was verified by repeating one condition for each of the three pairs shown in Fig. 2f five independent times (Extended Data Fig. 7a, c). The same preparations of nucleosome constructs and INO80 enzyme were used, although all subsequent steps were performed independently. However, swapping the Cy5 and Cy3 fluorophores between the two constructs in pair 1 (Extended Data Fig. 7b) required re-preparing of nucleosome constructs.

Direct reproducibility of smFRET experiments to measure looping kinetics (Fig. 1c) was limited to repeating the measurement once in the case of one of the sequences (Extended Data Fig. 3i). Our goal was to establish correlation between a large number of smFRET measurements on different sequences and their corresponding cyclizability values derived by loop-seq. Thus every time we performed a new smFRET experiment, we used a different sequence, rather than repeat an earlier measurement. High correlation between looping times measured via smFRET and cyclizability measured via the independent loop-seq method (Fig. 1f) establishes cyclizability as an accurate measure of looping time.

Reporting summary

Further information on research design is available in the Nature Research Reporting Summary linked to this paper.

Data availability

All sequencing data obtained as part of this study are deposited in the National Center for Biotechnology Information (NCBI) Sequence Read Archive (SRA) under accession number PRJNA667271. Nucleosome positions and NCP scores along the genome of *S. cerevisiae* as previously reported have been accessed from NCBI Gene Expression Omnibus (GEO) under accession number GSE36063. Nucleosome occupancy data in *S. cerevisiae* as previously reported have been accessed from NCBI GEO under accession number GSE97290. There are no restrictions on data availability. Source data are provided with this paper.

Code availability

No sequencing analysis in this study depends on the use of specialized code. Simple custom scripts were written in MATLAB (MathWorks) versions 9.0, 9.2, 9.4, 9.6 for analysis of sequencing data, and will be made available upon request. smFRET data acquisition was carried out by custom scripts that can be obtained from <http://ha.med.jhmi.edu/resources/> or upon request.

36. Nakano, M. et al. Single-molecule PCR using water-in-oil emulsion. *J. Biotechnol.* **102**, 117–124 (2003).
37. Langmead, B., Trapnell, C., Pop, M. & Salzberg, S. L. Ultrafast and memory-efficient alignment of short DNA sequences to the human genome. *Genome Biol.* **10**, R25 (2009).
38. Li, H. et al. The Sequence Alignment/Map format and SAMtools. *Bioinformatics* **25**, 2078–2079 (2019).
39. Mizuguchi, G., Wu, W.-H., Alami, S. & Luk, E. in *Methods in Enzymology* (eds. Wu, C. & Allis, C. D.) vol. 512, 275–291 (Academic Press, 2012).

Acknowledgements A.B. and T.H. thank C. Wu, X. Feng and M. F. Poyton for insights and help related to INO80 biochemistry, Q. Zhang for help with initial assay development efforts, and A. Biswas for providing passivated glass and quartz slides for smFRET experiments. K.P.H and S.E. thank M. Moldt for purification of recombinant INO80. This work was supported by the National Science Foundation grants PHY-1430124 and EFMA-1933303 (to T.H.), by the National Institutes of Health grants GM122569 (to T.H.), R01CA163336 (to J.S.S.) and GM130393 (to C.W.), by the European Research Council (Advanced Grant INO3D to K.P.H), and by the Deutsche Forschungsgemeinschaft (CRC1064 and Gottfried Wilhelm Leibniz-Prize to K.P.H). A.B. was a Simons Foundation Fellow of the Life Sciences Research Foundation. T.H. is an Investigator with the Howard Hughes Medical Institute.

Author contributions A.B. and T.H. designed the research. A.B. performed all aspects of the research and data analysis. A.B. and T.H. wrote the paper. Other authors contributed in the following areas: D.G.B. extracted nucleosome occupancy from published data and performed plectoneme density calculations. Z.Q. helped with the preparation of some libraries. T.K. and T.T.M.N. helped with initial assay development efforts and characterized RecBCD. A.R., S.E. and K.-P.H. purified INO80 and provided related insights. B.C. observed the phasing effect associated with a single biotin position. M.T.M. and C.W. assisted with the initial development of nucleosome-sliding assays. M.H., H.T.R. and J.S.S. assisted with initial analysis of sequencing data. All authors commented on the manuscript.

Competing interests The authors declare no competing interests.

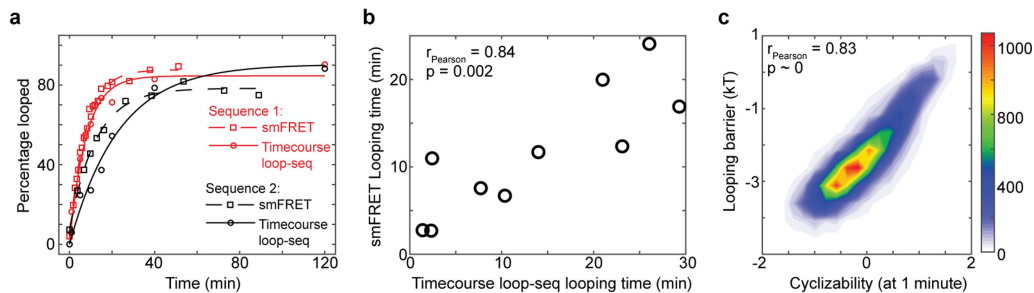
Additional information

Supplementary information is available for this paper at <https://doi.org/10.1038/s41586-020-03052-3>.

Correspondence and requests for materials should be addressed to T.H.

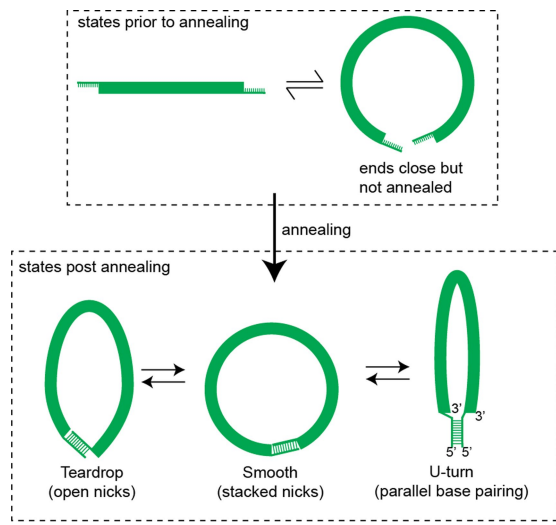
Peer review information *Nature* thanks Johan Elf, Wilma Olson and the other, anonymous, reviewer(s) for their contribution to the peer review of this work.

Reprints and permissions information is available at <http://www.nature.com/reprints>.

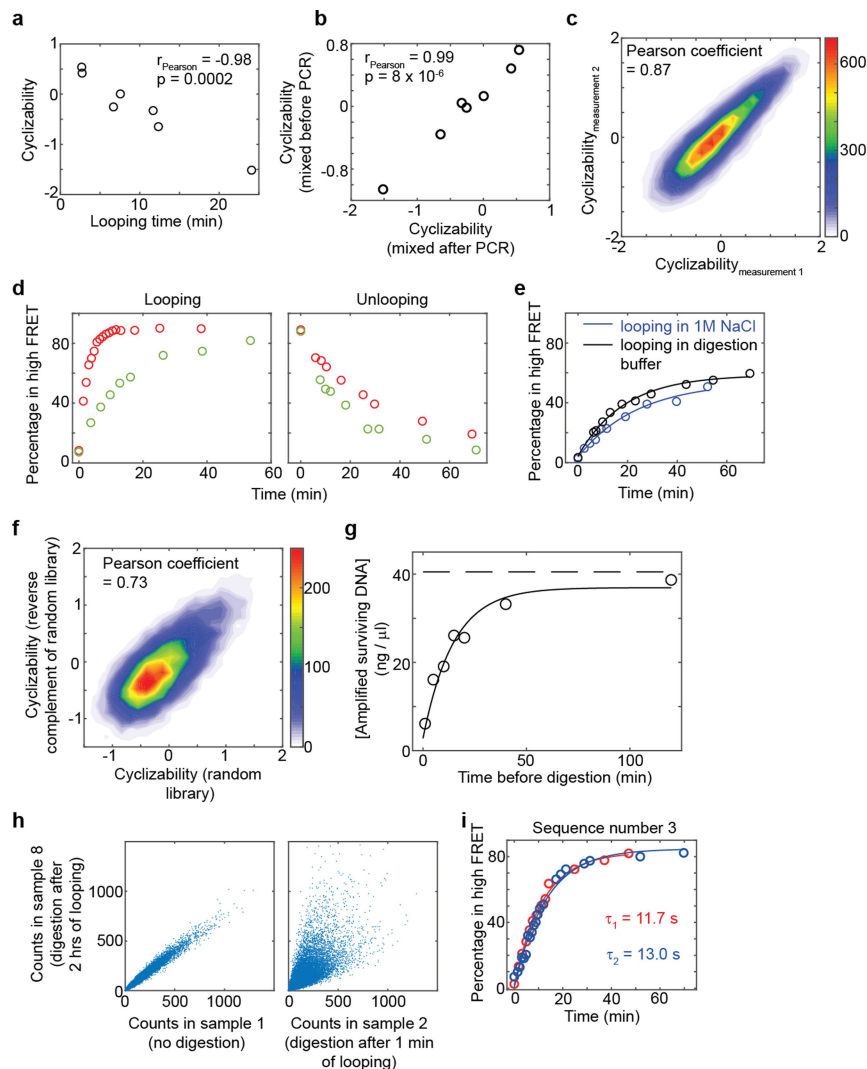


Extended Data Fig. 1 | Time course loop-seq. **a**, Looping kinetic curves of two individual sequences that were part of the cerevisiae nucleosomal library (Supplementary Note 4), obtained by performing two individual smFRET experiments (Fig. 1a–c) as well as timecourse loop-seq (Supplementary Note 3) on the library. **b**, Looping times of 10 sequences that were part of the cerevisiae nucleosomal library obtained from 10 individual smFRET experiments (Fig. 1c) versus looping times obtained by performing time-course loop-seq on the

library. Pearson's $r = 0.84$; 95% CI = 0.44, 0.96; $P = 0.002$, two-sided t -test. **c**, Looping barriers (natural logarithm of the looping times; see Supplementary Note 2) of all 19,907 sequences in the cerevisiae nucleosomal library obtained by performing time-course loop-seq versus the corresponding cyclizability values obtained by performing regular loop-seq involving 1 min of DNA looping before RecBCD digestion. Pearson's $r = 0.83$; 95% CI = 0.829, 0.837; $P < 0.00001$, two-sided t -test.



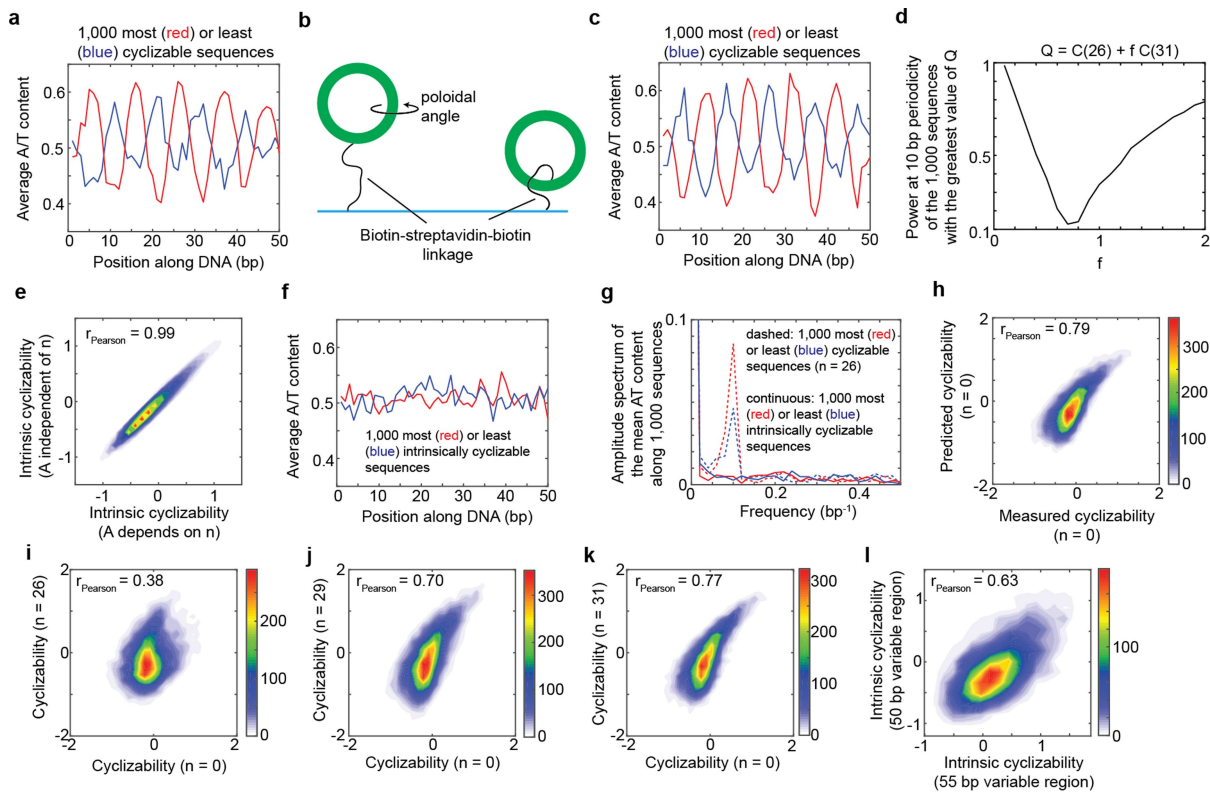
Extended Data Fig. 2 | Pre-looped and looped geometries. Before annealing of the ends, the DNA rapidly samples various configurations where the ends are far apart or closer together, described here for simplicity as a rapid equilibrium between two representative states. As previously described⁶, annealing captures the state in which the ends are close together. Thus, the rate of looping as measured in the FRET based assay reports on the equilibrium population fraction of the state where the ends are close but not annealed, irrespective of the exact shape and geometry of the subsequent annealed state. It thus addresses the biological question of how quickly regions of DNA can approach, which can then be stabilized by protein binding⁶. However, the formation of nucleoprotein complexes may require not just the ends to approach, but the intervening DNA to also adopt a certain shape, and the readout of looping rate does not distinguish between these possible shapes. Various shapes have been proposed for the subsequent annealed state, such as a teardrop configuration where the nicks are open and base-pair stacking across nicks is disrupted, and a smooth state in which base-pair stacking is preserved across the nicks¹¹. Other non-canonical geometries may also be possible, such as a U-turn geometry, where the sticky overhangs interact via reverse Watson–Crick base-pairing in a parallel stranded configuration. Conventional Watson–Crick base pairing between the overhangs, but in a geometry similar to the U-turn configuration, has been achieved in the past (hairpin loop¹⁰). Presence of mismatches or transient defects in the duplex region may influence whether such a geometry is preferred over the teardrop or smooth configuration¹⁰. Because all members of various libraries in our study used the same overhang sequences, relative differences between them in their looping kinetics are unlikely to be affected by a potential conformational heterogeneity of the looped state.



Extended Data Fig. 3 | See next page for caption.

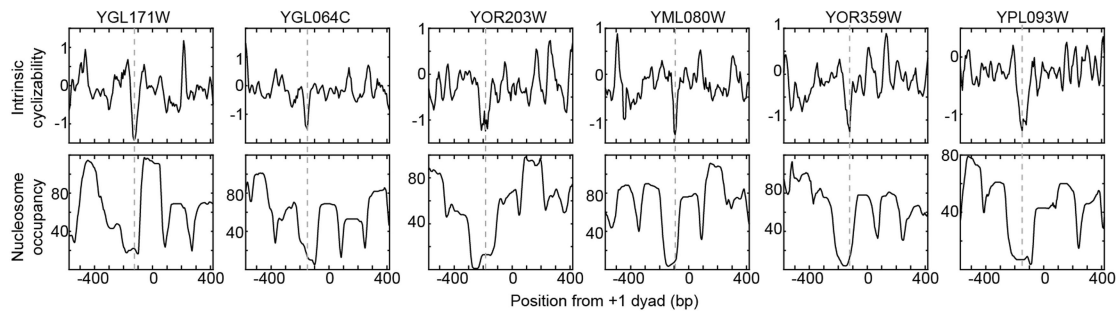
Extended Data Fig. 3 | Controls pertaining to the loop-seq assay. **a**, Seven of the ten sequences whose looping times were measured using smFRET (sequences 1–7 in Fig. 1c, and listed in Supplementary Note 1) were combined to form a small library. Plotted are the cyclizability values obtained by performing loop-seq on this library versus the looping times obtained from the individual smFRET experiments. Pearson's $r = -0.977$; 95% CI = $-0.848, -0.997$; $P = 0.0002$, two-sided t -test. This plot is similar to that in Fig. 1f, except that loop-seq was performed on a much smaller library comprising only these seven sequences. This control serves to revalidate the anti-correlative relation between looping time and cyclizability and confirm reproducibility of loop-seq measurements. **b**, Regular PCR of the entire library containing multiple templates can generate incorrectly annealed products that are annealed via the 25-bp identical adapters at the ends but have 50-bp bubbles in the middle. Such constructs would probably be extremely flexible and be protected from digestion owing to rapid cyclization. Emulsion PCR separates the templates in individual droplets, thereby preventing incorrect annealing between different templates. We performed a control experiment to verify that emulsion PCR of the library does not affect the measured value of cyclizability. In one case, seven template sequences (sequences 1–7 as listed in Supplementary Note 1 and Fig. 1c) were mixed and then a single round of ePCR was performed to form a small library. In another case, seven separate regular PCR amplifications were carried out for the seven template molecules. The amplified products were then mixed in equimolar proportions to form the library. Loop-seq was performed on these two 7-member libraries and two sets of cyclizabilities of the seven sequences were measured. As indicated, these values are highly correlated. Pearson's $r = 0.992$; 95% CI = $0.951, 0.999$; $P = 8 \times 10^{-6}$, two-sided t -test. **c**, Technical replicates of loop-seq performed on the cerevisiae nucleosomal library (Supplementary Note 4). Pearson's $r = 0.869$; 95% CI = $0.865, 0.872$; $P < 0.00001$, calculated using two-sided t -test. P value was obtained from a two-sided t -test. The same original library as provided by the manufacturer (Genscript) was used, but all subsequent steps were performed independently. **d**, This control was performed to verify the expectation that DNA sequences which are more bendable and thus loop quickly under high salt conditions are slow to unloop under low salt conditions. In red is the looping kinetics of sequence 6, and in green is that of sequence 7 (Fig. 1c) measured using smFRET. For the unlooping measurements, the slide containing nicked DNA was incubated for 2 h with high-salt imaging buffer containing 1 M NaCl. After that, low-salt imaging buffer containing no added NaCl was flowed in and the percentage of molecules in high FRET as a function of time was measured. **e**, This control was performed to verify that while performing loop-seq, molecules do not significantly unloop during the 20 min of digestion with RecBCD (Methods). If they do unloop, they would be immediately digested, which would affect the measurement of cyclizability. Sequence 5 (Supplementary Note 1) was used in this experiment. We find that digestion buffer (without the RecBCD enzyme) is in itself capable of looping molecules, and that too at a slightly faster rate than in the presence of looping buffer (which has 1 M NaCl, see Methods). This is owing to the presence of Mg²⁺ ions in the digestion buffer, which we know to also effect looping by allowing stable

hybridization of the ends⁶. Thus, molecules looped in the presence of 1 M NaCl in 1 min are expected to stay looped during the subsequent 20 min of digestion with RecBCD. **f**, This control was performed to understand the effect of the orientation of the central 50 bp sequence on the measured value of cyclizability. First the random library was constructed (where the sequence of DNA in the 50 bp central variable region are randomly selected; Supplementary Note 5). Then a library called 'mixed reverse complement of the random library and random library' was constructed by mixing the random library with another library, in which every sequences in the random library was present, but had its central 50-bp variable region flipped (Supplementary Note 6). Loop-seq was performed on this new library. We found that the cyclizability of a sequence represented in the Random Library half of this new library was correlated with that of the corresponding sequence in the other half, where the central 50-bp region was flipped. Pearson's $r = 0.73$; 95% CI = $0.72, 0.74$; $P < 0.00001$, calculated using a two-sided t -test. **g**, This plot serves to confirm the expectations that RecBCD does not digest looped molecules, and that over sufficient time, most molecules, even rigid ones, will loop. During time-course loop-seq (Supplementary Note 3), the original sample was split into eight identical fractions. Looping for various amounts of time and subsequent digestion was carried out for seven of the eight fractions, and one fraction was not subject to any digestion. All fractions were then PCR amplified (16 cycles) under identical conditions (see methods). Plotted are the concentrations of DNA obtained after PCR versus the corresponding times the samples were subject to the looping condition. These data points were fit to an exponential curve (solid line). The DNA concentration was obtained when no digestion was performed is represented as the dashed horizontal line. The fact that the fitted exponential approaches the dashed line indicates that for very long looping times, almost all molecules, even very rigid ones, have had sufficient time to loop and hence are protected from digestion. Thus, in this case, the concentration of DNA obtained after PCR of all surviving molecules approaches that of the fraction where no digestion was performed at all. Whether RecBCD would digest molecules sealed via non-canonical parallel base-pairing or other geometries (Extended Data Fig. 1) is not known. However, this control suggests that either it does not, or such unconventional base-pairings are rare. **h**, These plots serve to further demonstrate that if the library is permitted to loop for a very long time, most molecules, even very rigid ones, will loop, and that looped molecules are protected from subsequent digestion with RecBCD. In this case, the relative populations of various sequences measured after digestion should be similar to the case where no digestion was performed at all. We find this to indeed be the case: there is good correlation between the relative population of a sequence in sample 1 of time-course loop-seq (no digestion) and sample 8 (2 h of looping followed by digestion). However, correlation between the relative population of a sequence in sample 1 and that of a sequence in sample 2 (1 min of looping before digestion) is much weaker. This is because in sample 2, only those molecules whose sequences render them bendable enough to loop under 1 min are protected from subsequent RecBCD digestion. **i**, Technical replicates of the looping kinetic curve of sequence number 3 (Supplementary Note 1) measured using smFRET.



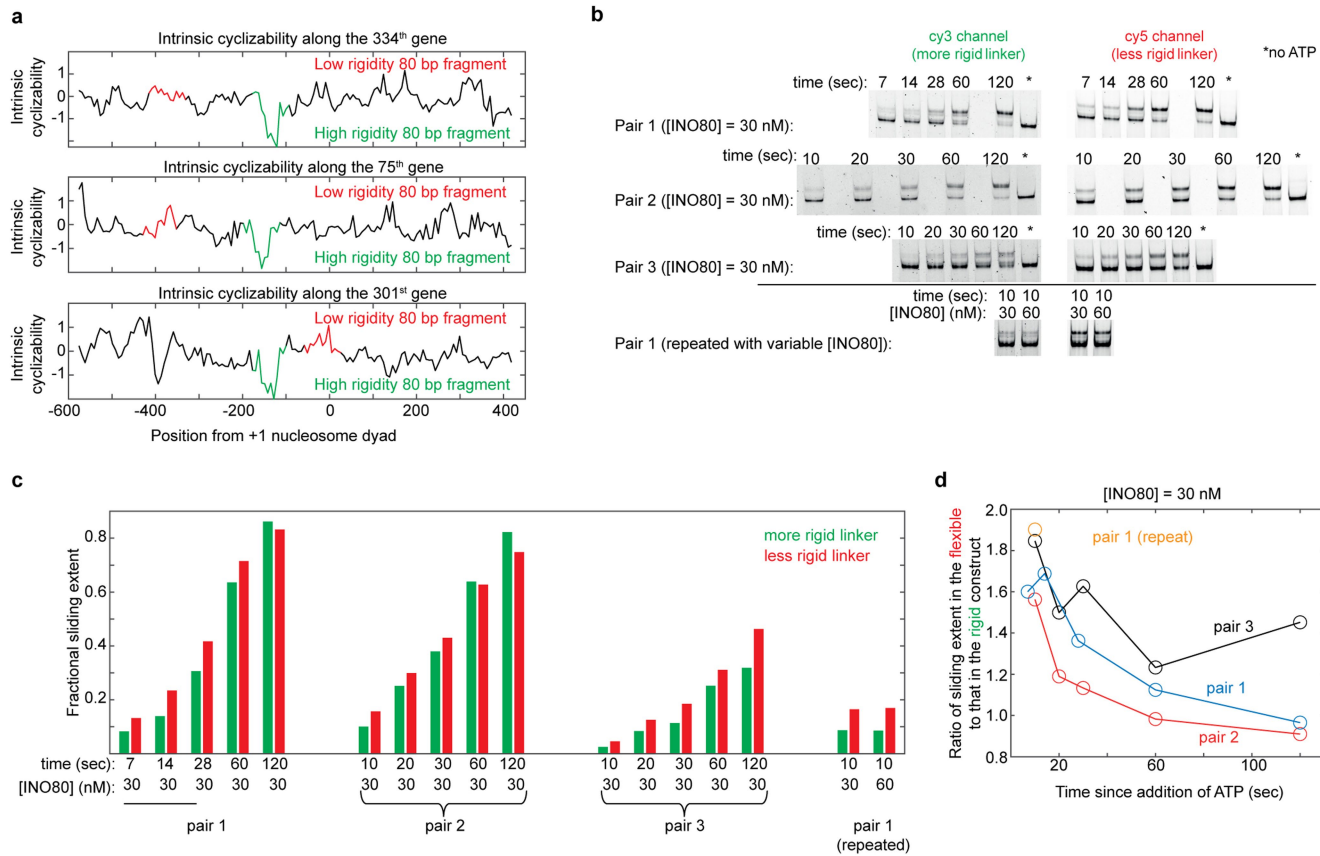
Extended Data Fig. 4 | Dependence of cyclizability on tether geometry and rotational phasing. **a**, Loop-seq was performed on the random library (Supplementary Note 5). Plotted is the mean A/T content as a function of position along the central variable 50 bp region, where the mean is calculated by averaging over the 1,000 most cyclizable (red) or least cyclizable (blue) sequences. The value of n ($n = 26$) is the distance in nucleotides of the biotin tether from the end of each molecule in the library (Fig. 1d). **b**, In an untethered geometry, sequence features such as the phase of the oscillations in A/T content may result in the looped configuration having a preference for a certain poloidal angle (rotation along the long axis of DNA). Preference for a certain poloidal angle translates to a preference for a certain orientation of the biotin-streptavidin tether. Shown above are two extreme cases—in one case, the poloidal angle preference of the sequence results in a preferential orientation of the tether on the outside, while in the other case, the tether points to the inside at the point of contact with the DNA. As the biotin-streptavidin-complex is quite large, the outside orientation may be more favoured for looping owing to steric considerations. The outside orientation can be converted to the inside orientation by moving the biotin tether point to a base that is half the DNA helical repeat away. This may explain why the phase of the oscillation of A/T content among the most or least cyclizable sequences shifts by half the helical repeat of DNA when the tether point is also shifted by half the helical repeat of DNA (about 5 bases) (compare **a** and **c**). **c**, The random library was re-prepared, placing the biotin 31 nucleotides away from the ends ($n = 31$) and loop-seq was performed. Plotted are the same quantities as in **a**, except the 1,000 most and least cyclizable sequences of the library were identified based on the newly obtained cyclizability values under the $n = 31$ condition. **d**, **e**, See context in which these panels are referred to in

Supplementary Note 7. In **e**, Pearson's $r = 0.987$; 95% CI = 0.986, 0.987; $P < 0.00001$, two-sided t -test. **f**, Mean A/T content as a function of position along the variable region of the random library, where the averaging is done over the 1,000 sequences that have the highest (red) or lowest (blue) values of intrinsic cyclizability. The scale of the axes is the same as in **a** and **c**. **g**, Amplitude spectra obtained from the fast Fourier transforms of the plots in **f** (solid lines) and **a** (dashed lines). **h**, 2D histogram of the scatter plot of measured cyclizability of sequences in the random library prepared with the biotin at the very end of the molecule ($n = 0$ condition) vs its predicted value based on the oscillatory model (equation (1) in Supplementary Note 7). Pearson's $r = 0.787$; 95% CI = 0.78, 0.793; $P < 0.00001$, two-sided t -test. **i–k**, 2D histogram of scatter plot of measured cyclizabilities of sequences in the random library prepared at $n = 0$ vs prepared at $n = 26, 29, 31$ nucleotides. In **i**, Pearson's $r = 0.38$; 95% CI = 0.37, 0.40; $P < 0.00001$, two-sided t -test. In **j**, Pearson's $r = 0.70$; 95% CI = 0.69, 0.71; $P < 0.00001$, two-sided t -test. In **k**, Pearson's $r = 0.77$; 95% CI = 0.76, 0.78; $P < 0.00001$, two-sided t -test. **l**, The use of long 10-nucleotide overhangs has been shown to eliminate the need for ligase and to reduce the dependence of looping on rotational phasing between the ends⁶. Shown here is a 2D histogram of the scatter plot of intrinsic cyclizability of a sequence in the random library (which had 50 bp of DNA along the central variable region) versus the corresponding sequence in library L (Supplementary Note 8), in which 5 bases were added to the variable region. A correlation coefficient only slightly poorer than the correlation between cyclizability values of the random library and the reverse complement of the random library (Extended Data Fig. 3f) suggests that rotational phasing of the ends does not significantly influence intrinsic cyclizability. Pearson's $r = 0.63$; 95% CI = 0.61, 0.65; $P < 0.00001$, two-sided t -test. See Supplementary Note 8.



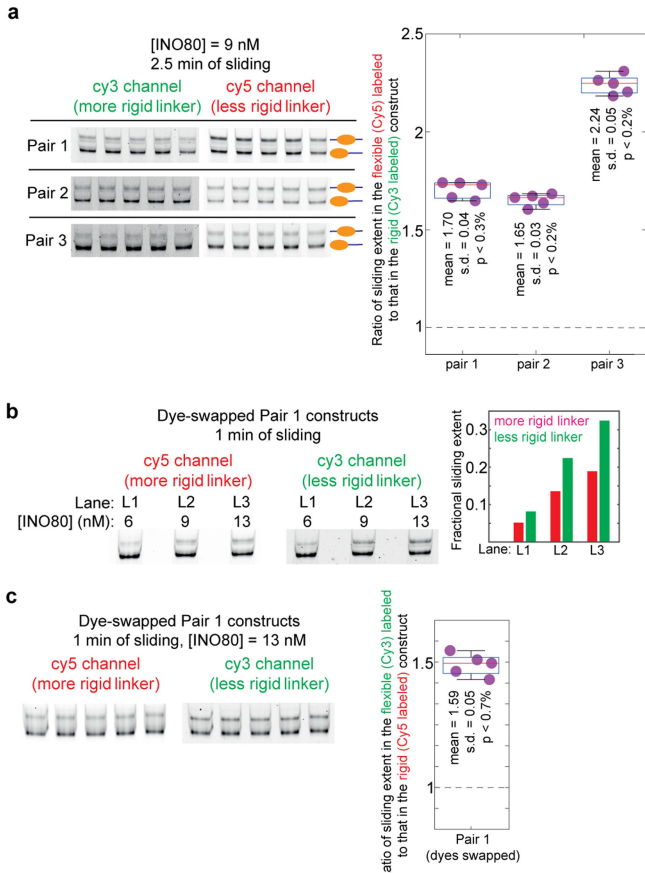
Extended Data Fig. 5 | Intrinsic cyclizability and nucleosome occupancy vs position from the dyads of the +1 nucleosomes of various individual genes in *S. cerevisiae*. Plots are as shown for the two individual genes in Fig. 2c. The dashed line marks the ordinate value where intrinsic cyclizability is lowest.

Article



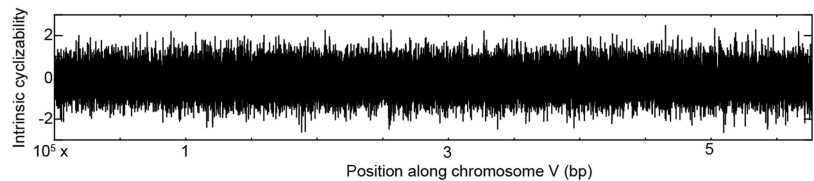
Extended Data Fig. 6 | DNA pair selection and timecourse of INO80 remodelling. **a**, Intrinsic cyclizability as a function of position from the +1 nucleosomal dyad, along the 334th, 75th and 301st genes in the list of 576 genes along which intrinsic cyclizability was measured (Supplementary Note 9). The 80-bp linker regions of both constructs (with rigid and flexible linkers extending from the 601 sequence) in pairs 1, 2 and 3 along which INO80 sliding extent was measured, were selected from the 334th, 75th, and 301st genes respectively. Genes are oriented in the upstream to downstream direction. Red and green denote the selected 80-bp less rigid and more rigid linker regions, respectively. See Supplementary Note 11. **b, c**, The remodelling reactions shown in Fig. 2f were all performed for 1 min of remodelling, under various enzyme concentrations. Here we show, instead, remodelling reaction time courses at saturating concentrations of INO80 for all three pairs. Conditions are identical to Fig. 2f, except that saturating (30 nM) INO80 is used and remodelling is permitted to progress for various amounts of time after addition of ATP (Methods). In all cases, the two constructs in a pair are present

simultaneously, and distinguished by imaging the gel once for Cy3 and once for Cy5 fluorescence. Thus, although the sliding extent can be very sensitive to sliding time (especially for short sliding times), robust comparisons of sliding extents can be made between the two constructs in a pair. Quantification is as described in Supplementary Note 11. Sliding on the constructs in pair 1 was repeated in a separate experiment in presence of 30 nM enzyme, and also side by side in presence of 60 nM enzyme. Near identical extents of sliding indicate saturation has been reached at 30 nM INO80. **d**, Ratio of the fractional sliding extent in the construct formed on the more flexible linker to that formed on the more rigid linker, at various time points since addition of ATP, and in presence of 30 nM INO80. The dashed line indicates a ratio of 1. The ratio is computed from the data in **b**. The extent of sliding under saturating enzyme conditions is consistently higher for the construct involving more flexible linker (except, as expected, when the sliding extent approaches 100%). Solid lines connect observations that were made from the same initial reaction volume by sampling its fractions at various time points.

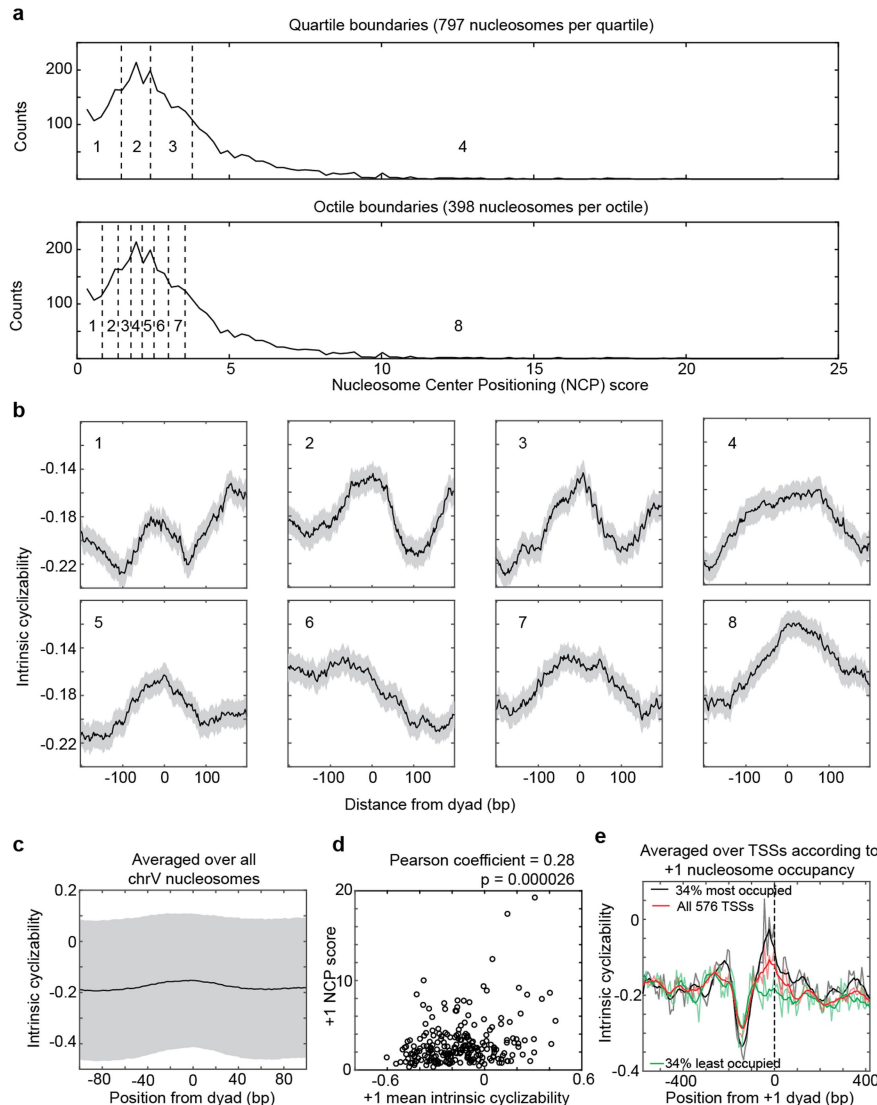


Extended Data Fig. 7 | Control experiments pertaining to the INO80-mediated sliding of nucleosomes. **a.** To assess our confidence in the result that INO80 mediated sliding is greater in the construct with the less rigid linker, we performed nucleosome-sliding experiments similar to those reported in Fig. 2f five times for each pair in the presence of 9 nM INO80 and for 2.5 min of sliding. These constitute technical replicates. The products of sliding were analysed on a 6% TBE gel as done in Fig. 2f. Each gel was imaged separately for Cy3 and for Cy5 fluorescence and quantified to calculate the fold difference in sliding extent between the flexible and the rigid construct in each pair. The measurements of fold-differences for each pair are displayed in the box plots, along with the actual data points. The central mark in each box (red) represents the median and the bottom and edges represent the 25th and 75th percentile respectively. The whiskers extent to the most extreme datapoints. Also indicated are the mean and s.d., and upper limit of the *P* value (defined here as the probability of obtaining a fold-difference of 1 if the distribution of fold differences has the same mean and s.d. as that of these 5 measurements) as obtained by the application of Chebyshev's inequality. Dashed line represents a fold-difference of 1. **b.** In the experiment described in Fig. 2f, the more rigid construct in all pairs was labelled with Cy3, while the less rigid construct was labelled with Cy5. This control verifies that the result that sliding extent is greater in the less rigid construct is not influenced by different dye properties. We swapped the dyes between the two constructs in pair 1. We then performed nucleosome-sliding experiments on this modified pair 1 constructs for the three INO80 concentrations that yielded detectable sliding in Fig. 2f (6, 9, 13 nM), and for 1 min of sliding as in Fig. 2f. The products of sliding were analysed on a 6% TBE gel, and the sliding extents quantified as in Fig. 2f. We indeed find that even when the dyes are swapped, sliding extent is greater for nucleosomes formed on the less rigid construct. **c.** To obtain better statistics of sliding along the dye-swapped pair 1 constructs, we repeated one of the conditions in **b** (13 nM INO80, 1 min of sliding) five times. These constitute technical replicates. The measured fold-difference values are displayed in the box plot. The central mark in each box (red) represents the median and the bottom and edges represent the 25th and 75th percentile respectively. The whiskers extent to the most extreme datapoints. Also indicated are the mean, s.d. and upper limit of the *P* value (defined as in **a**) as obtained by the application of Chebyshev's inequality. Dashed line represents a fold difference of 1.

Article



Extended Data Fig. 8 | Intrinsic cyclizability along *S. cerevisiae* chromosome V at 7 bp resolution. Data were obtained by performing loop-seq on the chromosome V library (Supplementary Note 12).

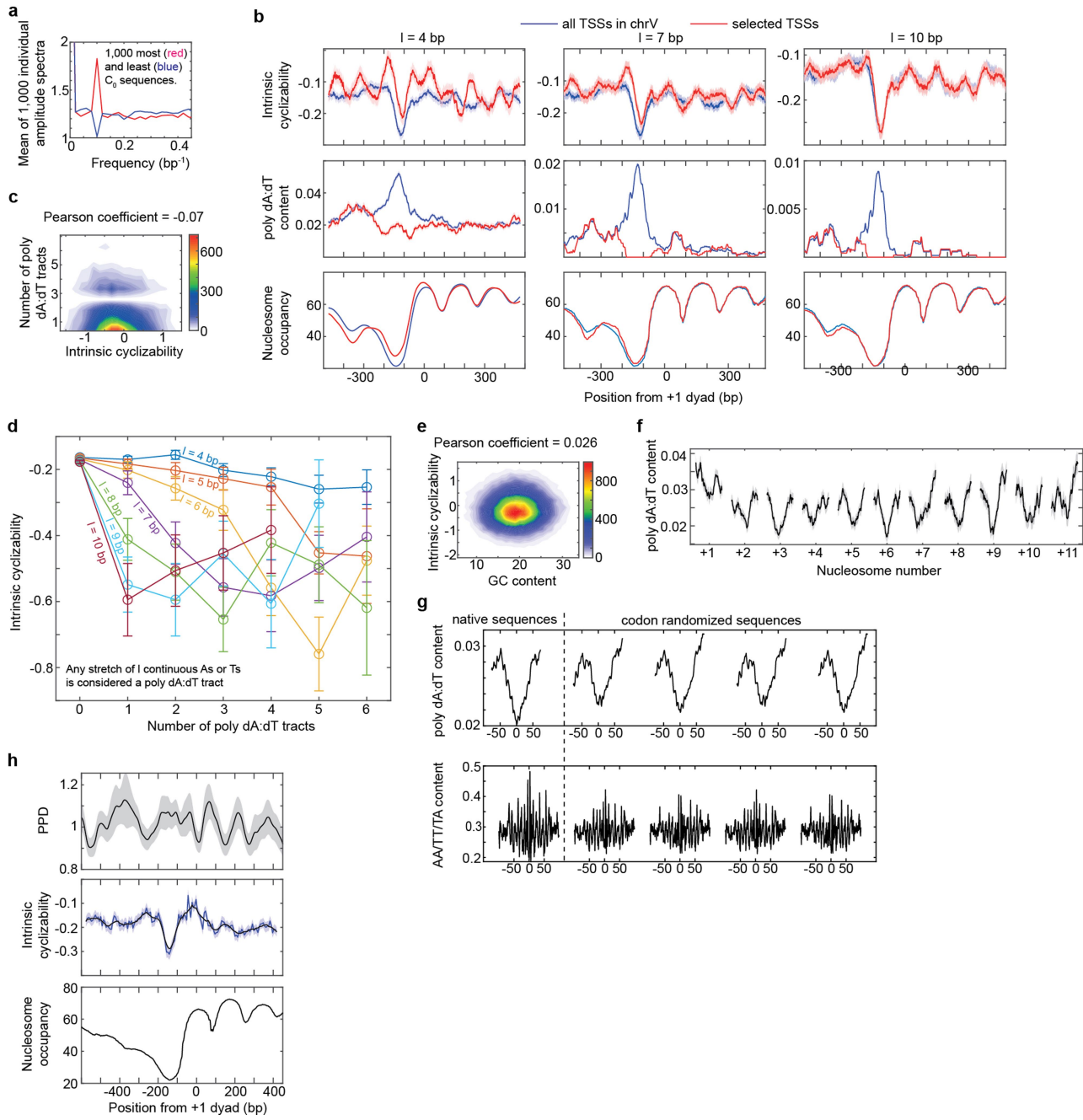


Extended Data Fig. 9 | Intrinsic cyclizability along nucleosomes.

a, Distribution of NCP scores³³ of all 3,192 *S. cerevisiae* chromosome V nucleosomes. Quartile and octile boundaries of the distribution are shown as dashed lines and numbered (1 to 4 for quartiles and 1 to 8 for octiles). **b**, Mean intrinsic cyclizability of DNA as a function of position from the dyads of nucleosomes along yeast chromosome V, averaged over nucleosomes in each octile indicated in **a**. Error extents (shaded background) are s.e.m. **c**, Mean intrinsic cyclizability as a function of position, averaged over all 3,192 *S. cerevisiae* chromosome V nucleosomes (solid line). Height of the shaded region is the standard deviation of measurements. **d**, Scatter plot of the NCP scores of the 227 +1 nucleosomes of the 227 genes identified along chromosome V vs the

mean intrinsic cyclizabilities of DNA along the 147 bp that span these nucleosomes. Intrinsic cyclizability values were obtained by performing loop-seq on the chromosome V library. Pearson's $r = 0.28$, 95% CI = 0.15, 0.39. $P = 2.6 \times 10^{-5}$, t -test, two-sided. **e**, Plot of intrinsic cyclizability as a function of position along all the 576 genes in the tiling library (red), and among 34% of these genes that had the highest (black) or lowest (green) NCP score value of the gene's +1 nucleosome. Plots were obtained in a manner identical to that in Fig. 2b. Intrinsic cyclizability on either side of the dyad of +1 nucleosomes of genes that have high +1 nucleosome NCP score (black) is asymmetric, being higher on the TSS proximal (that is, 'left') side of the dyad.

Article



Extended Data Fig. 10 | See next page for caption.

Extended Data Fig. 10 | Loop-seq measurements compared to expectations based on earlier measurements and models. **a**, Two sets of 1,000 plots each of A/T content as a function of position along the central 50 bp variable region of 1,000 sequences in the random library with the highest and lowest values of intrinsic cyclizability were generated. Fast Fourier transforms of these two sets of 1,000 plots were taken individually and used to calculate a total of 2,000 amplitude spectra. Plotted is the mean of the 1,000 amplitude spectra for the 1,000 sequences that have the highest (red) or lowest (blue) intrinsic cyclizability values. The plot indicates that sequences that have very high or low intrinsic cyclizabilities also tend to be characterized by enhanced or suppressed periodic modulations in AT content respectively at the DNA helical repeat. **b**, We consider a poly(dA:dT) stretch which has at least l consecutive A or T nucleotides to be a poly(dA:dT) tract. For various values of l , plotted are intrinsic cyclizability (top), poly(dA:dT) tract content (middle), and nucleosome occupancy (bottom) vs position from the dyad of the +1 nucleosome, averaged over all 227 identified genes in *S. cerevisiae* chromosome V (blue) or over a selected subset of genes that show no peak in poly(dA:dT) content at the NDR (red; 30%, 62%, and 86% of genes for $l=4$ bp, 7 bp, 10 bp respectively). See Supplementary Note 15 for plotting details, including how poly(dA:dT) content is defined. **c**, 2D histogram of the scatter plot between the number of poly(dA:dT) tracts in the 50 bp variable region and intrinsic cyclizability of sequences in the chromosome V library. Any stretch of l or more consecutive As or Ts (here $l=4$) is considered a poly(dA:dT) tract. Thus a sequence with one stretch of 5 As, and no other As or Ts, in the 50 bp variable region has 2 poly(dA:dT) tracts if l is considered to be 4. The scatter plot indicates that the overall correlation between intrinsic cyclizability and poly(dA:dT) content is very poor. Only non-overlapping sequences in the chromosome V library were considered. Pearson's $r=-0.07$. 95% CI = -0.09, -0.05. $P < 0.00001$, t -test, two-sided. **d**, Binned histogram of the data in **c** (which represents the $l=4$ bp case), as well as for more restrictive definitions of poly(dA:dT) stretches ($l=5$ to 10 bp). The y-axis values are the mean intrinsic cyclizabilities of those sequences in the chromosome V library that contain the number of poly(dA:dT) tracts in the central 50 bp variable region as specified along the x-axis. Error bars are s.e.m. For $l=4$, there were $n=5,081, 2,801, 1,705,$

948, 521, 268, 170 non-overlapping sequences in the chromosome V library which had a poly(dA:dT) content of 0, 1, 2, 3, 4, 5, 6 respectively. For $l=5$, the corresponding N values were 8,771, 1,594, 695, 323, 150, 89, 36. For $l=6$, the corresponding N values were 10,523, 655, 295, 117, 62, 25, 32. For $l=7$, the corresponding N values were 11,203, 290, 109, 56, 27, 30, 16. For $l=8$, the corresponding N values were 11,497, 109, 58, 23, 30, 17, 11. For $l=9$, the corresponding N values were 11,608, 57, 23, 29, 19, 13, 7. Because the count of poly(dA:dT) = 6 is less than 10, this point was left out from the plot. For $l=10$, the corresponding N values were 11,665, 23, 30, 21, 11, 6, 1. Again, the intrinsic cyclizability for poly(dA:dT) content = 5, 6 were left out from the plot because the n value for these were less than 10. **e**, 2D histogram of the scatter plot of mean GC content along the central 50 bp variable region of sequences in the chromosome V library vs their intrinsic cyclizabilities. Pearson's $r=0.026$. 95% CI = 0.019, 0.033. $P < 0.00001$, t -test, two-sided. **f**, A plot of mean poly(dA:dT) content ($l=4$) as a function of position around the dyads of gene-body nucleosomes along chromosome V in *S. cerevisiae*. The points along the horizontal axis where the nucleosome categories (+1, +2, and so on) are marked represent the dyads of the nucleosomes. Light shaded region represents s.e.m. Poly(dA:dT) content was calculated as described in Supplementary Note 15. **g**, Mean poly(dA:dT) content ($l=4$) and AA/TT/TA vs position along the native and codon-randomized nucleosomal DNA sequences of the same 500 +7 nucleosomes along which intrinsic cyclizability profiles are reported in Fig. 3g. **h**, Predicted plectoneme density (PPD) (see Supplementary Note 16) (top), intrinsic cyclizability (middle) and nucleosome occupancy (bottom) vs position from the +1 nucleosomal dyad, averaged over all 576 genes in the tiling library (Supplementary Note 9). PPD along each gene was first smoothed using a rolling window of 51 bp. The smoothed PPDs were then averaged at each position across all 576 genes, normalized by the mean, and plotted as the solid line in the top panel. The shaded background represents s.e.m. Intrinsic cyclizability and nucleosome occupancy were plotted as in Fig. 2b. For the plot of intrinsic cyclizability, the solid blue and black lines represent data without and with a 7-fragment smoothing respectively (as in Fig. 2b). The shaded blue background represents s.e.m. of intrinsic cyclizability values in the unsmoothed data.

Corresponding author(s): Taekjip Ha

Last updated by author(s): Oct 9, 2020

Reporting Summary

Nature Research wishes to improve the reproducibility of the work that we publish. This form provides structure for consistency and transparency in reporting. For further information on Nature Research policies, see our [Editorial Policies](#) and the [Editorial Policy Checklist](#).

Statistics

For all statistical analyses, confirm that the following items are present in the figure legend, table legend, main text, or Methods section.

n/a Confirmed

- The exact sample size (n) for each experimental group/condition, given as a discrete number and unit of measurement
- A statement on whether measurements were taken from distinct samples or whether the same sample was measured repeatedly
- The statistical test(s) used AND whether they are one- or two-sided
Only common tests should be described solely by name; describe more complex techniques in the Methods section.
- A description of all covariates tested
- A description of any assumptions or corrections, such as tests of normality and adjustment for multiple comparisons
- A full description of the statistical parameters including central tendency (e.g. means) or other basic estimates (e.g. regression coefficient) AND variation (e.g. standard deviation) or associated estimates of uncertainty (e.g. confidence intervals)
- For null hypothesis testing, the test statistic (e.g. F , t , r) with confidence intervals, effect sizes, degrees of freedom and P value noted
Give P values as exact values whenever suitable.
- For Bayesian analysis, information on the choice of priors and Markov chain Monte Carlo settings
- For hierarchical and complex designs, identification of the appropriate level for tests and full reporting of outcomes
- Estimates of effect sizes (e.g. Cohen's d , Pearson's r), indicating how they were calculated

Our web collection on [statistics for biologists](#) contains articles on many of the points above.

Software and code

Policy information about [availability of computer code](#)

Data collection	smFRET data acquisition was carried out by custom scripts that can be obtained from " http://ha.med.jhmi.edu/resources/ " or upon request.
Data analysis	No sequencing analysis in this study depends on the use of specialized code. Bowtie 1 and SAMtools were used to analyze sequencing data. Simple scripts written in MATLAB (Matworks) versions 9.0, 9.2, 9.4, 9.6 were also used and will be made available upon request.

For manuscripts utilizing custom algorithms or software that are central to the research but not yet described in published literature, software must be made available to editors and reviewers. We strongly encourage code deposition in a community repository (e.g. GitHub). See the Nature Research [guidelines for submitting code & software](#) for further information.

Data

Policy information about [availability of data](#)

All manuscripts must include a [data availability statement](#). This statement should provide the following information, where applicable:

- Accession codes, unique identifiers, or web links for publicly available datasets
- A list of figures that have associated raw data
- A description of any restrictions on data availability

All sequencing data obtained as part of this study are deposited in the National Center for Biotechnology Information (NCBI) Sequence Read Archive (SRA) under accession number PRJNA667271. Nucleosome positions along the genome of *S. cerevisiae* as reported earlier have been accessed from NCBI Gene Expression Omnibus (GEO) under accession number GSE36063. Nucleosome occupancy data in *S. cerevisiae* as reported earlier have been accessed from NCBI GEO under accession number GSE97290. Figs. 1 - 4, as well as Extended Data Figs. 2-5, 8-10 have associated raw data. There are no restrictions on data availability.

Field-specific reporting

Please select the one below that is the best fit for your research. If you are not sure, read the appropriate sections before making your selection.

Life sciences

Behavioural & social sciences

Ecological, evolutionary & environmental sciences

For a reference copy of the document with all sections, see nature.com/documents/nr-reporting-summary-flat.pdf

Life sciences study design

All studies must disclose on these points even when the disclosure is negative.

Sample size

For all loop-seq measurements, the number of different sequences in a library was largely determined by the available options as provided by the library manufacturer (Genscript). The manufacturer offered two library sizes: 12,472 sequences or 92,918 sequences. Accordingly, for most libraries used in this study, the number of sequences were close to either of these two numbers. The only exception was the Cerevisiae Nucleosomal Library, where two libraries (each ordered using the 12,472 size option) were mixed to construct the final 19,907 sequence library. This number reflects the number of nucleosomal DNA fragments over which we could measure intrinsic cyclizability. The various N values for the number of nucleosomes in each category (-9 through +9) in Fig. 4 merely reflects how many such nucleosomes were present in the library.

In the Tiling library, tiling each gene at a resolution of 1 bp would have covered just a few genes, given the limitation of library size. Further, we did not want to tile every 5 or 10 bp, because of potential phasing effects owing to the helical repeat. Hence, two viable options were 3 bp and 7 bp. We chose 7 bp to allow us to cover more genes. Given the library size (92,918) this limited us automatically to 576 genes. A few spots were still free, which we filled in with other test/ trial sequences.

Likewise, in the case of the ChrV library, we chose yeast chromosome V because upon tiling it at 7 bp resolution, the number of resulting fragments would be close to the library size limit. The number of genes and nucleosomes over which data have been averaged in Fig. 3 are not selected, but merely reflect the genes and nucleosomes present along yeast chromosome V.

In the case of Library L, we chose 500 nucleosomes to randomize gene sequences along, reflecting the fact that in the tiling library, there were ~500 genes we had measured flexibility along, and the averaging was sufficient to see distinct intrinsic cyclizability peaks associated with the 500 +1 nucleosomes. As described above, tiling was done at a resolution of 7 bp. Remaining spots in the library were filled with other sequences for important control experiments, as described in Supplementary Note 14.

The number of DNA fragments for which we measured smFRET looping times (Fig. 1c) was so chosen, so as to sufficiently cover the broad range of intrinsic cyclizability values of sequences in the Cerevisiae Nucleosomal Library (Fig. 1f).

For sliding experiments involving INO80, we chose to perform the experiment on 3 pairs of constructs. We were not attempting to build quantitative kinetic models for how intrinsic cyclizability influences sliding rate. Our goal was to consistently ascertain whether rigid DNA hinders INO80 sliding. We did so by measuring sliding rates on these three pairs under various conditions of [INO80], sliding time, or dye labeling strategies (Fig. 2f, Extended Data Figs. 6, 7). The low-throughput nature of these measurements, the high costs associated with trying out each new pair of sequences, and the nature of our goals, lead to us limiting the number of different pairs to 3.

Data exclusions

No data were excluded.

Replication

All presented loop-seq data in figures (unless explicitly comparing between multiple loop-seq runs on the same library, as in Extended Data Fig. 3c) were compiled from a single run of loop-seq on the library in question. However, some sequences in every library were included as part of at least one other library. Pearson's coefficient of correlation for the intrinsic cyclizability values of these common sequences (and the 95% confidence interval and p values), as obtained via the two independent loop-seq runs on the two libraries, was measured to confirm reproducibility (Extended Data Fig. 3a-c, Supplementary Notes 4, 5, 6, 9, 12, 14). All such pearson's correlation coefficients were greater than or similar to the correlation coefficient of cyclizability values of the two sets of reverse complement sequences in the "Mixed Reverse Complement of the Random Library and the Random Library" (Extended Data Fig. 3f). Further, measurements of intrinsic cyclizabilities of common sequences in different libraries constitute completely independent measurements starting from independently purchased libraries from the manufacturer.

All Pearson's r have been calculated using the corrcoef function in MATLAB (Matworks). For two random variables A and B, Pearson's r is the covariance of A and B, divided by the product of their standard deviations. p values have always been calculated using the MATLAB (matworks) function corrcoef, which calculated the p value by transforming the correlation to create a t-statistic having n-2 degrees of freedom, where n is the number of measurements. The test was always two-sided. Further, extremely small p values have always been indicated as $p < 0.00001$.

Reproducibility of the result that nucleosome sliding by INO80 is favored by flexible linker DNA was verified by repeating one condition for each of the three pairs shown in Fig. 2f 5 independent times (Supplementary Note 7). The same preparation of nucleosomes were used, though all subsequent steps were independent for these 5 replicates. Further, swapping the Cy3 and Cy5 dyes in one of the pairs required re-preparing the nucleosome constructs.

Direct reproducibility of smFRET experiments to measure looping kinetics (Fig. 1c) was limited to repeating the measurement once in the case of one of the sequences (Extended Data Fig. 3i). Our goal was to establish correlation between a large number of smFRET measurements on different sequences and their corresponding cyclizability values derived by loop-seq. Thus every time we performed a new smFRET experiment, we used a different sequence, rather than repeat an earlier measurement. High correlation between looping times measured via smFRET and cyclizability measured via the independent loop-seq method (Fig. 1f) establishes cyclizability as an accurate measure of looping times.

Randomization

There was no allocation of samples into experimental groups, and hence the question of whether such allocation was random or not does not arise.

Blinding

There was no subjective investigation involved, or any investigation that could be influenced by bias. All results were derived from sequencing data, which is publicly available. Also, there was no group allocation involved, and so the question of whether investigators were blinded to it or not does not arise.

Reporting for specific materials, systems and methods

We require information from authors about some types of materials, experimental systems and methods used in many studies. Here, indicate whether each material, system or method listed is relevant to your study. If you are not sure if a list item applies to your research, read the appropriate section before selecting a response.

Materials & experimental systems

- | | |
|-------------------------------------|-------------------------------|
| n/a | Involved in the study |
| <input checked="" type="checkbox"/> | Antibodies |
| <input checked="" type="checkbox"/> | Eukaryotic cell lines |
| <input checked="" type="checkbox"/> | Palaeontology and archaeology |
| <input checked="" type="checkbox"/> | Animals and other organisms |
| <input checked="" type="checkbox"/> | Human research participants |
| <input checked="" type="checkbox"/> | Clinical data |
| <input checked="" type="checkbox"/> | Dual use research of concern |

Methods

- | | |
|-------------------------------------|------------------------|
| n/a | Involved in the study |
| <input checked="" type="checkbox"/> | ChIP-seq |
| <input checked="" type="checkbox"/> | Flow cytometry |
| <input checked="" type="checkbox"/> | MRI-based neuroimaging |